IEEE Access
Multidisciplinary ⋮ Rapid Review ⋮ Open Access Journal

Received 23 April 2024, accepted 25 May 2024, date of publication 28 May 2024, date of current version 5 June 2024.

Digital Object Identifier 10.1109/ACCESS.2024.3406434

RESEARCH ARTICLE

Stability Improvement of Sulselrabar System With Integrated Wind Power Plant Using Multi-Band PSS3C Based Mayfly Optimization Algorithm

MUHAMMAD RUSWANDI DJALAL, IMAM ROBANDI, AND MOHAMAD ALMAS PRAKASA
Department of Electrical Engineering, Institut Teknologi Sepuluh Nopember, Surabaya 60111, Indonesia

Corresponding author: Imam Robandi (robandi@ee.its.ac.id)

This work was supported in part by the Institut Teknologi Sepuluh Nopember through its Indonesian Education Scholarships, and in part by the Education Fund Management Institute (LPDP) and the Higher Education Funding Center (BPPT) Kemendikbudristek.

ABSTRACT The introduction of additional controllers is essential in modern electric power systems to enhance their stability, particularly during disturbances. One effective method is the implementation of power system stabilizers (PSS). However, precise coordination of PSS equipment is necessary to determine the optimal locations and parameters. This study focuses on the optimal analysis of Multi-Band PSS3C (MB-PSS3C) coordination in integrated Wind Power Plant (WPP) systems in South, Southeast, and West Sulawesi (Sulselrabar). An artificial intelligence approach, utilizing the Mayfly Optimization Algorithm (MOA), is suggested for optimizing both the location and parameters of the PSS. Comparative investigations were conducted to assess the efficacy of MB-PSS3C in comparison with SB-PSS1A and MB-PSS2B, based on previous research. The performance analysis employed the time domain simulation method, reviewing the speed deviation response, field voltage response, PSS output voltage response, and rotor angle response for each generator. Eigenvalue analysis was performed for each control scheme. Load changes were applied to generators 1 (BAKARU) and 11 (WPP SIDRAP) to evaluate the performance of the system. The application of the MOA-based MB-PSS3C results in an increased damping ratio, improved speed response, and a more optimal rotor angle. MB-PSS3C provides a larger additional damping signal to the generator exciter, as indicated by the increase in the field voltage on the generator.

INDEX TERMS Stability, multi-band PSS3C, wind power plant, mayfly optimization algorithm, Sulselrabar.

I. INTRODUCTION

An electrical power system is a multifaceted infrastructure comprising components for energy production, delivery, processing, and consumption [1]. Operating a power system to minimize costs ensures steady supply of electricity at an appropriate voltage and frequency [2]. Stability is crucial for ensuring dependability of electric power systems during disruptions [3]. These disturbances can range from minor fluctuations in generation and load to more significant events, such as faults. Transient stability refers to the power system's ability to maintain synchronization after a significant disruption [4].

Oscillations within a power system manifest at various frequency modes. The local mode is responsible for the oscillation of a power plant generator relative to other generators in the same system [5]. Concurrently, the swing of one generator in relation to another in a different area is associated with the inter-area mode [6]. When the frequency falls between 0.01 and 0.05 Hz, all swinging generators are connected to the global mode [7]. This oscillation mode can have significant adverse effects, such as constraining the transmission capacity or disrupting loads. Therefore, mitigating these oscillations is crucial for facilitating efficient network operation and planning.

The associate editor coordinating the review of this manuscript and approving it for publication was Ruisheng Diao.

Reducing the system instability is essential for ensuring efficient power system planning and operation because of the significant influence of these oscillations. Control methods such as Flexible AC Transmission Systems (FACTS) [8], [9], Static Synchronous Compensator (STATCOM) [10], [11], Static Var Compensator (SVC) [12], [13], [14], and Power System Stabilizer (PSS) [15], [16] have been employed to enhance system stability. In particular, the PSS is effective in reducing the relative power angle oscillations and speed changes, thereby improving the overall power system stability. By adding damping torque to the excitation system, PSS efficiently mitigates disturbance-induced oscillations [17].

There are two varieties of PSS: Single Band (SB-PSS) and Multi Band (MB-PSS) [18]. The PSS type used in the industry was standardized by IEEE [19], [20]. A PSS controller sends an additional signal to the Automatic Voltage Regulator (AVR) of a synchronous generator to reduce power oscillations [21], [22]. After a disturbance, certain components of the electrical torque changes align with the rotor speed fluctuations and rotor angle variations (synchronization torque), contributing to the overall damping torque. The use of a very quick AVR can significantly reduce the damping torque, and as a result, this torque turning negative could intensify power fluctuations instead of damping them [23]. The application of a PSS provides torque damping to maintain the dynamic stability in an electric power system [24]. Compared with the standard PSS, the dual-input MB-PSS offers higher stability and versatility in controlling various oscillation modes [25], [26]. MB-PSS, based on three correlated bands, includes a gain, filter, and limiter in each band, intended for different oscillation modes [20]. The generator active power and speed fluctuations served as inputs to the MB-PSS [27].

The application of conventional SB-PSS1A significantly enhances the stability of multi-machine systems. In [28], the transient stability of an IEEE 9-bus system was examined during disturbances at various bus locations. The incorporation of PSS1A reduced the power-angle oscillations and settling times in the system. When PSS1A is combined with a generator and excitation system, it improves the overall stability of the system. In [29], PSS1A was utilized to enhance transient stability in a two-area, four-engine system. Particle Swarm Optimization (PSO) is employed to modify PSS1A settings, reduce oscillations and improve stability. With ideal parameter tuning, PSS1A proved effective in enhancing the stability of an the IEEE 14-Bus system [30]. The analysis evaluates the time-domain behavior of the system following a disturbance, demonstrating improved stability using the pole placement and system participation factor methodologies. In [31], the Firefly Algorithm (FA) was used as the optimization approach, applying PSS1A to a multi-machine system in South, Southeast, and West Sulawesi (Sulselrabar). The application results showed an improvement in the frequency stability and rotor angle performance of the system.

MB-PSS successfully suppresses low-frequency oscillations (LFOs) and enhances small-signal stability in a multi-machine power system. Additionally, it can reduce the drift in the engine speed [32]. In a previous study [33], the coordination of MB-PSS2B and SVC resulted in increased damping and enhanced stability in the eigenvalue system, generator speed response, field voltage, and rotor angle of the Sulselrabar system. The ideal parameters for MB-PSS2B and SVC were determined using the Mayfly Optimization Algorithm (MOA). In [34], MB-PSS2B and a thyristor controlled series capacitor (TCSC) compensator were employed to increase the stability margin of the power system. The coordination of the TCSC compensator with the multi-objective PSO algorithm using the Integral Time Absolute Error (ITAE) was implemented. This study demonstrated the efficient reduction of power oscillations in a two-area four-engine system through the synchronization of TCSC and MB-PSS2B.

Researchers introduced MB-PSS type PSS3C (MB-PSS3C) into this system. In an effort to reduce electromechanical swings in the Polish Power System (PPS), a study [35] utilized multi-criteria optimization for PSS3C parameters, employing Genetic Algorithms (GA) to minimize the objective function. The computations demonstrated the successful reduction of electromechanical swings through the application of multi-criteria optimization on PSS3C. In another study [36], disturbances related to the rotor angle stability, such as power distribution oscillations and rotor speed variations, were discussed. This study examined the effect of PSS3C on attenuating these oscillations. The synchronous generator field flux is provided by the ST5B static excitation system, and PSS3C's extra stabilizing signals enhance engine damping performance. The Downhill Simplex Algorithm was employed to adjust the PSS3C settings, resulting in increased voltage stability and reduced oscillations in the rotor angle. Using a different approach [37], Model Predictive Control (MPC) was explored as a potential PSS. This study employs a numerical optimization approach to determine the optimal control outputs while considering system restrictions. The multi-machine system with four engines and two areas utilizes the designed MPC. The controller was tested under three faults: a quick shift in the voltage reference, a transmission line outage, and a three-phase fault. The MPC performs well in managing restrictions and various types of oscillation dampers. Study [38] reports improvements to the excitation system of the 1400 MW Tehri-Koteshwar Hydro Power Plant to address active power oscillations. This involved the use of an over excitation limiter (OEL) in conjunction with PSS3B. The study in [39] focused on damping active power oscillations in a hydro power plant using PSS3B. To ensure stability during transient disturbances, the excitation system and the PSS collaborate to maintain the system voltage within predefined bounds. In an extensive study [40], the PSS4C architecture was introduced as a control approach using real-time estimates of the center-of-inertia velocity derived from large-area measurements. A reduced-order two-area test case was used to study this phenomenon.

In recent decades, substantial efforts from researchers, electricity planners, and renewable energy operators have been directed towards enhancing the quality of electricity systems. With its developed infrastructure, advanced technology, and relative affordability, wind energy has gained popularity among renewable sources. However, integrating wind energy into at power system network can be challenging owing to its natural fluctuations [41], [42], [43]. In [44], the transient voltage stability of a power system with high Wind Power Plant (WPP) penetration was investigated, focusing on the IEEE 14 Bus case. A high WPP penetration can result in reliability restrictions, frequency stabilization, and voltage instability [42]. The report briefly summarizes research on load frequency control and advocates the use of FACTs devices, Energy Storage Systems (ESS), and high-voltage direct current (HVDC) linkages as potential solutions for future issues. In another study [45], the voltage stability in electric power systems integrating more wind energy was examined. This study investigates the influence of increasing doubly fed induction generator-based wind energy conversion system (DFIG-WECS) integration in the IEEE 14 Bus system. Active power-voltage (PV) analysis identifies constraints on the voltage stability.

The inclusion of renewable generation sources, including WPP, presents challenges in maintaining Power Quality (PQ) and stability in electric power system. These difficulties stem from the erratic and variable generation of these sources [46], [47]. The effective coordination of control devices is essential for mitigating the impact of WPP penetration. A comprehensive review in [48] covered a range of conventional and adaptive algorithms employed for controlling FACTS devices, including the STATCOM. The objective is to enhance the power quality of utility networks that experience WPP penetration. The research described in [49] provides a thorough examination of the impact of Battery Energy Storage Systems (BESS) on primary frequency control delivery to support the growing ubiquity of WPP in IEEE 9-bus systems. The simulation results show that the BESS can reduce the system oscillations after disruptions. In [50], a hybrid control methodology that combine fuzzy logic and nonlinear sliding mode control (FL-NLSM) was proposed. This hybrid control approach, utilizing the unique qualities of both FL and NLSM, improves the damping properties of the system response and addresses nonlinearity, especially when there is uncertainty regarding the parameters. The hybrid control technique specifically addresses the significant variability of renewable energy sources, such as wind power, and variations in load requirements.

In [51], the impact of uncertainty on a multi-machine power system with a high penetration rate of the WPP was investigated. The proposed solution is a Fuzzy Type II-based PSS1A aimed at reducing uncertainty and increasing the dynamic stability margin in the integrated system of a WPP multi-machine two areas. In [52], a new sparsity-promoting adaptive control technique was presented to configure PSS1A settings in a 39-bus system with 10 machines and an integrated wind farm. The simulation findings confirm that the proposed approach improves the ability of the PSS to damp oscillations and enhances its resistance to variations in wind energy. The study in [53] examined the effect of wind energy on the stability of small signals in electric power networks. The combination of AVR and PSS1A was considered effective in mitigating undesirable changes. The acquired data demonstrate that the suggested combination has a beneficial effect on the stability of DFIG-based wind farms connected to the IEEE 39 Bus System, even under typical operational conditions. In [54], improvements in LFO damping were presented for IEEE 39 Bus systems with WPP penetration through a robust coordinated control strategy involving PSS1A and Power Oscillation Damper (POD). The simulation results demonstrated enhanced damping with the proposed control strategy across various operating scenarios, including line faults and outages under different loading conditions. The paper [55] provides a comprehensive analysis of the Multi-Band PSS type 4C (MB-PSS4C) based on PSO connected to the ST1A excitation system. Different levels of WPP penetration were integrated into the network and then examined. These findings illustrate that connecting MB-PSS4C to ST1A effectively stabilizes the system.

The Sulselrabar system incorporates various types of generators including thermal power plants, hydro power plants, and WPP. Preliminary studies have assessed the system's performance both before and after the integration of the WPP. In [56], the optimal power flow in the Sulselrabar system was discussed for both scenarios by, employing a PSO-based optimization. The objective is to enhance the line losses and voltage on each bus within the system. Another study [57] focused on analyzing the small-signal stability in the Sulselrabar system following WPP integration. The findings revealed oscillations in the frequency and rotor speed as a consequence of integrating the WPP into the system.

The application of MB-PSS in several previous studies has demonstrated optimal system stability, whether in single-machine infinite bus (SMIB) or multi-machine example systems, as well as in real-world systems. The utilization of MB-PSS, incorporating a combination of shaft speed deviation input and changes in electrical power, proved to be more advantageous than SB-PSS. This is crucial for analyzing real-world applications and providing valuable insights for evaluations by electricity managers. In a previous study [33], the application of the MB-PSS, specifically the PSS2B type, was proposed for the Sulselrabar system. PSS2B represents an evolution of MB-PSS, following the previous version, SB-PSS type PSS1A. Currently, several types of MB-PSS exist, including PSS3C. The Sulselrabar system is a complex multi-machine system that is currently undergoing continuous development. Consequently, a persistent stability study is essential, particularly in the context of applying MB-PSS3C to the system. This constitutes our main motivation for

introducing a novel control scheme that utilize MB-PSS3C for the Sulselrabar system.

In a previous study [33], the implementation of MB-PSS used in the Sulselrabar system before WPP integration involved 37 buses, comprising 28 buses at 150 kV, 7 buses at 70 kV, and 2 buses at 30 kV. Currently, the number of buses has increased to 46, with 36 buses at 150 kV, 8 buses at 70 kV, and 2 buses at 30 kV. Updating these data is crucial for observing the latest phenomena in the system, especially concerning the system stability. This forms our second motivation for proposing a new system structure with WPP integration into the Sulselrabar system.

Artificial intelligence (AI) technology, based on machine learning [58], [59] and, swarm intelligence [60], has been used to assist researchers in optimizing complex dynamic systems. Previous studies on PSS optimization have utilized optimization methods such as FA [31] and PSO [61]. Both FA and PSO are optimization techniques based on swarm intelligence. However, the recently introduced MOA outperformed both the FA and PSO in benchmarking results [62]. Furthermore, MOA have proven to be effective in optimizing power systems, consistently yielding optimal results. In [63], MOA was employed to facilitate the coordination and tuning of parameters for the PSS auxiliary damping controller simultaneously. Another study [64] presented an MOA approach to optimize the performance of a three-phase active power filter by setting the gain of a proportional-integral-derivative (PID) controller. In [65], a practical technique was described that uses MOA to optimize the PID parameters of a hydro-turbine governor, thereby improving the governor system's performance. In our earlier work [33], we used the MOA to optimize the SVC and MB-PSS2B parameters to enhance the stability of the Sulselrabar system. The MOA operates based on the Comprehensive Damping Index (CDI) objective function, which maximizes the damping system. The results highlighted the optimal placement and parameters for SVC and MB-PSS2B. Our third motivation for applying the MOA approach is to optimize the parameters and locations of MB-PSS3C in the Sulselrabar system, combined with a WPP system, owing to its exceptional performance.

Table 1 highlights the current research gaps by providing a comprehensive overview of the techniques and conclusions of various studies. It also facilitates a comparison between previous research endeavors and the current study. The primary contributions of this study are as follows:

1) The installation of MB-PSS3C is proposed to enhance the stability of the Sulselrabar integrated WPP system by updating the data system.
2) The MOA method was implemented to optimize both the location and parameters of MB-PSS3C in Sulselrabar, integrated with a WPP system.
3) Exploring the deployment of MB-PSS3C through damping analysis, time-domain simulation, and eigenvalue analysis. This entails scrutinizing responses such as the Speed Deviation, Field Voltage, PSS Output Voltage, and Rotor Angle to evaluate the system's performance.

TABLE 1. A comparative analysis between prior research and the proposed work.

Ref	Controller	Method	Remarks
Implementation of SB & MB-PSS on Example & Real System			
[28]	PSS1A	-	IEEE 9 Bus
[29]	PSS1A	PSO	Two Area Four Engine System
[30]	PSS1A	S-Domain	IEEE 14 Bus
[31]	PSS1A	Firefly	Sulselrabar System Without WPP
[33]	PSS2B	MOA	Sulselrabar System Without WPP
[34]	PSS2B	PSO	Two Area Four Engine System
[35]	PSS3C	GA	Polish Power System (PPS)
[36]	PSS3C	Down-hill Simplex	SMIB
[37]	PSS4C	-	Two Area Four Engine System
[38]	PSS3C	-	Tehri–Koteshwar Hydro Power Plant
[39]	PSS3C	-	Hydro Power Plant
[40]	PSS4C	-	Two Area Four Engine System
WPP Penetration Control			
[45]	FACTS: TCSC	-	IEEE 14 Bus System With WPP
[48]	FACTS: STATCOM	-	A Comprehensive Review
[49]	BESS	-	IEEE 9 Bus System With WPP
[50]	FL-NLSM	-	IEEE 9 Bus System With WPP
[51]	PSS1A	Fuzzy Type 2	Multi-Machine Two Area Integrated WPP
[52]	PSS1A	Adaptive Control Method	IEEE 39 Bus System With WPP
[53]	AVR-PSS1A	-	IEEE 39 Bus System With WPP
[55]	PSS4C	PSO	Multi-Machine Two Area Integrated WPP
[66]	FACTS: STATCOM	-	A Comprehensive Review
Proposed Research			
The Current Research	MB-PSS3C	MOA	Optimizing the placement and sizing of the MB-PSS3C in the Sulselrabar system, which includes a WPP, and updating the data system.

The article is structured as follows: Section II presents models for electric power systems and an overview of mathematical models for PSS. Section III outlines the research methodology, and Section IV presents the results. Finally, Section V concludes the research.

II. SYSTEM MODEL

This section discusses system modeling, encompassing aspects such as generator models, excitation system models, and stabilizer system models.

A. GENERATOR MODEL

To enhance the observation of the system's response, the linear equation representing the synchronous generator can be articulated in the matrix model of Equation (1), as shown at the bottom of the page [67], where the following symbols denote specific parameters:

V_D, V_Q	: Stator voltage components along the d-q axis.
V_F	: Rotor Field Voltage.
V_D, V_Q	: Rotor voltage components along the d-q axis.
r	: Stator Resistance.
L_d, L_q	: Rotor inductance components along the d-q axis.
$\lambda_{q0}, \lambda_{d0}$	: Initial flux components along the d-q axis.
KMF	: Rotating Magnetic Field.
M_D, M_Q	: Mutual Inductance.
$\Delta I_d, \Delta I_q$	: Stator current components along the d-q axis.
ΔI_F	: Rotor Field Current.
$\Delta I_D, \Delta I_Q$	: Rotor current components along the d-q axis.
$\Delta\omega$	: Generator Speed Change.
$\Delta\delta$	: Generator rotor angle change.

B. EXCITATION SYSTEM AND STABILIZE MODEL

Before reaching a steady state, the operating point of the generator changes in response to load variations, as indicated by the oscillation frequency and rotor angle. The system enters an unstable state when rapid oscillations occur, and certain exciters do not respond sufficiently quickly to halt them. To mitigate these problems, a brief exciter was applied to enhance the damping of the system oscillations during the early swing condition following a disturbance. Torque attenuation is hampered by negative damping, which can be reduced using this type of exciter. Equation (2) provides the formula for the fast exciter [68].

$$E_{fd} = K_A \left(V_t - V_{ref}\right) / \left(1 - T_A s\right) \tag{2}$$

The time constant is denoted as T_A, and the gain is represented by K_A. Owing to equipment limitations, the exciter output must be confined within the range $V_{Rmin} < E_{fd} < V_{Rmax}$. A block diagram illustrating the fast exciter is shown in Fig. 1. V_t represents the output of the terminal voltage transducer and V_{ref} represents the intended value of the stator terminal voltage.

The magnitude of the change in the mechanical torque T_m depends on the speed drop constant, transfer function of the governor, and energy source. Changes in T_m values are induced by alterations in speed, load, and speed reference (Governor Speed Changer-GSC). A block schematic of the governor model is shown in Fig. 2 [69].

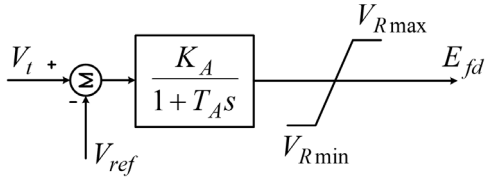

FIGURE 1. Exciter model.

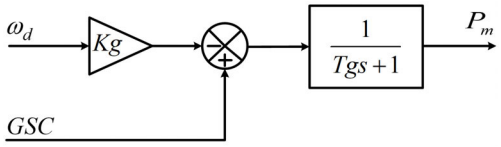

FIGURE 2. Governor model.

The mechanical torque is denoted by T_m, and the speed change is represented by d. The governor time constant is denoted as T_g, droop-governor constant is represented by R,

$$\begin{bmatrix} \Delta v_d \\ -\Delta v_F \\ 0 \\ \Delta v_q \\ 0 \\ \Delta T_m \\ 0 \end{bmatrix} = - \begin{bmatrix} r & 0 & 0 & \omega_0 L_q & \omega_0 k M_Q & \lambda_{q0} & 0 \\ 0 & r_F & 0 & 0 & 0 & 0 & 0 \\ 0 & 0 & r_D & 0 & 0 & 0 & 0 \\ -\omega_0 L_d & -\omega_0 k M_F & -\omega_0 k M_D & r & 0 & -\lambda_{d0} & 0 \\ 0 & 0 & 0 & 0 & r_Q & 0 & 0 \\ \frac{\lambda_{q0} - L_d i_{q0}}{3} & \frac{-k M_F i_{q0}}{3} & \frac{-k M_D i_{q0}}{3} & \frac{-k M_Q i_{d0}}{3} & \frac{k M_Q i_{d0}}{3} & -D & 0 \\ 0 & 0 & 0 & 0 & 0 & -1 & 0 \end{bmatrix} \begin{bmatrix} \Delta i_d \\ \Delta i_F \\ \Delta i_D \\ \Delta i_q \\ \Delta i_Q \\ \Delta\omega \\ \Delta\delta \end{bmatrix}$$
$$- \begin{bmatrix} L_d & k M_F & k M_D & 0 & 0 & 0 & 0 \\ k M_F & L_F & M_R & 0 & 0 & 0 & 0 \\ k M_D & M_R & L_D & 0 & 0 & 0 & 0 \\ 0 & 0 & 0 & L_q & k M_Q & 0 & 0 \\ 0 & 0 & 0 & k M_Q & L_Q & 0 & 0 \\ 0 & 0 & 0 & 0 & 0 & -\tau_j & 0 \\ 0 & 0 & 0 & 0 & 0 & 0 & 1 \end{bmatrix} \begin{bmatrix} \Delta \dot{i}_d \\ \Delta \dot{i}_F \\ \Delta \dot{i}_D \\ \Delta \dot{i}_q \\ \Delta \dot{i}_Q \\ \Delta\dot{\omega} \\ \Delta\dot{\delta} \end{bmatrix} \tag{1}$$

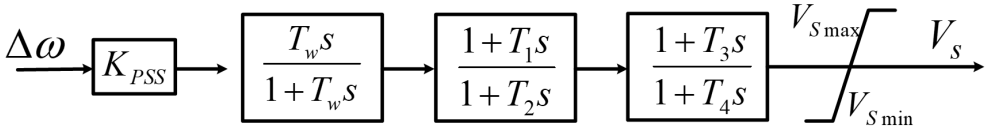

FIGURE 3. PSS1A model.

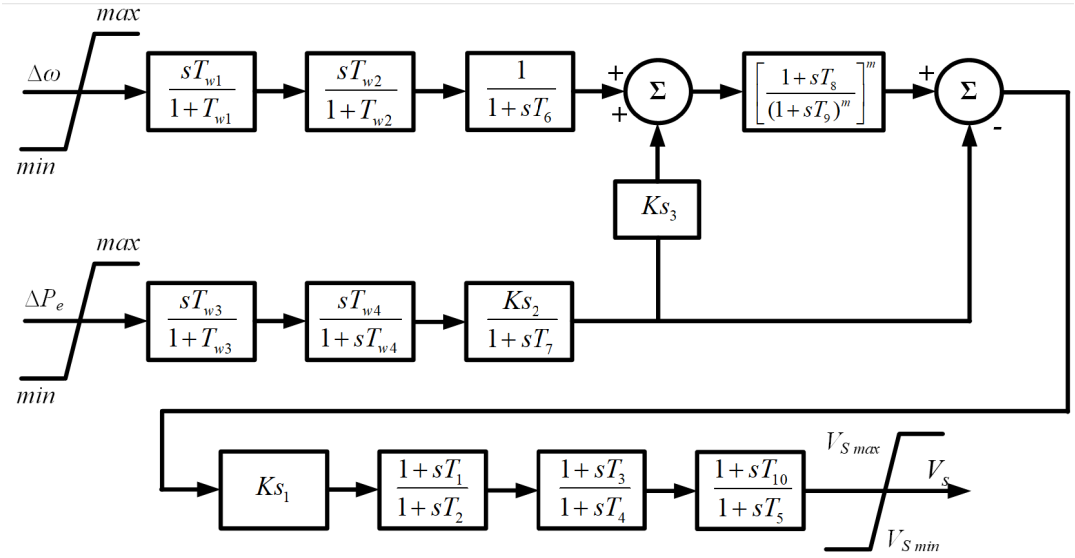

FIGURE 4. MB-PSS2B model.

and gain constant is K_g ($1/R$). In this governor model, it is assumed that the Governor Speed Changer (GSC) is set to 0. Equation (3) describes the mechanical power of the governor as a result of the cooperation between the speed governor and the turbine system.

$$P_m = -\left[\frac{K_g}{1+T_g s}\right]\omega_d \tag{3}$$

C. PSS MODEL

PSS enhances the electromechanical oscillation damping of the generator. Although the generator's power and speed may fluctuate during this stabilization process, they typically remain within a steady-state functioning range. Equation (4) illustrates how the swing equation expresses the relationship between the aforementioned components, and it transforms into Equation (5) for small disturbances:

$$\frac{2H}{\omega_0}\frac{d^2\delta}{dt} = \bar{T}_m - \bar{T}_e - K_D\Delta\bar{\omega}_r \tag{4}$$

$$\Delta T_e = T_s\Delta\delta + T_D\Delta\omega \tag{5}$$

Equations (4) and (5) provide insights into the changes in torque values. A positive T_s value implies that the synchronization torque component opposes the change in the rotor angle, resulting in a decrease in the torque when the rotor angle increases. Similarly, for positive T_D values, the torque damping component opposes changes in the rotor speed. In summary, stability is achieved when both T_s and T_D are positive, whereas instability or oscillation occurs when T_s is positive and T_D is negative.

The rotor's angle is denoted by δ, its angular fundamental speed by ω, and its angular speed by ω_r. The change in electric torque, denoted as T_e, represents the electrical torque, while T_m represents the mechanical torque. The synchronization coefficient is denoted as T_s, T_D represents the damping coefficient, and H is the inertia constant with K_D. The change in rotor angle is indicated by $\Delta\delta$, while the change in speed is represented by $\Delta\omega$ [70].

The modeling of SB-PSS1A is shown in Fig. 3 [71]. In the diagram, the washout filter is denoted as T_w, the output PSS as Vs, and the lead-lag gains as T_1, T_2, T_3, and T_4, with limitations set by V_{Smax} and V_{Smin}. The PSS improves the damping of the system by supplying additional signals to the generator excitation system. The gain served as an amplifier to quantify the damping effect introduced by the PSS. In control systems, the washout function (T_w) is commonly employed to mitigate or minimize the influence of low-frequency signals, thereby enabling the system to respond more efficiently to dynamic changes. Lead-lag compensators (T_1, T_2, T_3, T_4) are utilized to manipulate the frequency response of a system, addressing the phase lag concerns introduced by specific components in this scenario. The limiter is implemented to ensure that the PSS output (V_s) stays within predefined limits, preventing undesirable system behavior.

Fig. 4 depicts the two-input MB-PSS2B model. In contrast to SB-PSS, MB-PSS was developed to address the notable

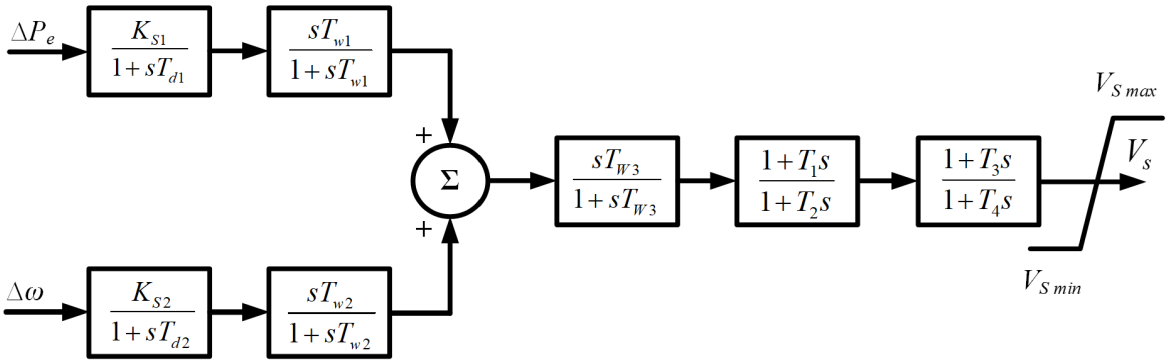

FIGURE 5. MB-PSS3C model.

drawback of SB-PSS. SB-PSS may introduce signal noise into the system, potentially causing excessive modulation in the excitation system and introducing a reference error. The potential causes of this noise are torsional oscillations owing to changes in the electrical torque or lateral motion of the shaft. This noise negatively affects the excitation and electric torque of the generator. To address these issues, transitioning from a traditional single-input PSS to a multi-input PSS such as the MB-PSS is necessary. The inputs for the MB-PSS include changes in the generator's electrical power (ΔP_e) and rotor angle velocity ($\Delta\omega$). These input signals are processed through circuits that include the transducer and washout. The transducer converts incoming impulses into voltage signals and the washout circuit maintains the output of the stabilizer in a continuous state. The MB-PSS model was developed from IEEE-type PSS2B, as illustrated in Fig. 4. Each input signal undergoes meticulous processing through transducer circuits and washout circuits (T_{w1}-T_{w4}), as indicated by T_6-T_7. The temporal constants T_8 and T_9, representing the torque filters, are crucial in determining the response of the system to changes in electrical power and rotor angle velocity.

The MB-PSS3C model with dual inputs is depicted in Fig. 5, where the first input is the rotor speed and the second is the electrical power. The washout filter is characterized by the time constants T_{W1}, T_{W2}, and T_{W3}, and the transducer by T_{d1} and T_{d2}, with gains K_{s1} and K_{s2}. Adjusting the gain and filter coefficients to generate a signal that is proportional to the acceleration power requires changes in the polarity and proportion of the input signal. In the filter block, the appropriate parameter values (T_1-T_4) were selected to provide the necessary phase adjustment. IEEE proposed PSS3C as an enhanced version of PSS3B, incorporating the ability to disable PSS at low turbine power. Terminal voltage transducers sense the terminal voltage, filter it to the DC magnitude, and load compensators maintain a constant voltage level at locations other than the generator terminals. These are essential components of the excitation system. Partial correction of the transformer impedance is advantageous for efficiently regulating the voltage at a point in the center of the step-up transformer when two or more synchronous generators are connected to a bus via separate transformers.

D. SULSELRABAR SYSTEM

This study utilizes the most recent data from the Sulselrabar system, encompassing 15 generators, 57 transmission lines connecting major load centers, and the latest daily operational data. The system operates at a voltage of 150 kV and is compriseds of 46 buses. Fig. 6 illustrates at single-line diagram of the Sulselrabar system. Bus numbering was essential for the analytical process. Table 2 presents a list of the bus numbers for the Sulselrabar system.

TABLE 2. Numbering of sulselrabar system generations.

Bus	Name-Type	Bus	Name-Type
1	Bakaru-Slack	24	Bontoala-Load
2	Pinrang Generator	25	Panakukkang-Load
3	Suppa Generator	26	Tanjung Bunga-Load
4	Tello Generator	27	Sungguminasa-Load
5	Borongloe Generator	28	Talasa-Load
6	PLTUjnpto Generator	29	Jeneponto-Load
7	PLTUpngya Generator	30	Bulukumba-Load
8	PLTUbsw Generator	31	Bone-Load
9	Bantaeng Generator	32	Soppeng-Load
10	Sinjai Generator	33	Sidrap-Load
11	WPPsidrap Generator	34	Maros-Load
12	Sengkang Generator	35	Bolangi-Load
13	Palopo Generator	36	Enrekang-Load
14	Makale Generator	37	Siwa-Load
15	Mamuju Generator	38	Pangkep70-Load
16	Polmas-Load	39	Tonasa-Load
17	Majene-Load	40	Mandai-Load
18	Pare-Pare-Load	41	Daya-Load
19	Barru-Load	42	Tello70-Load
20	Pangkep-Load	43	Tello Lama70-Load
21	Bosowa-Load	44	Bontoala 70-Load
22	Kima-Load	45	Tello30-Load
23	Tello Lama-Load	46	Barawaja-Load

III. RESEARCH METHOD

This section describes the proposed technique for MB-PSS3C placement and parameter optimization, providing a comprehensive exploration of its methodology and application. Additionally, it explains the implementation of the method and elucidates the objective function used for the optimization.

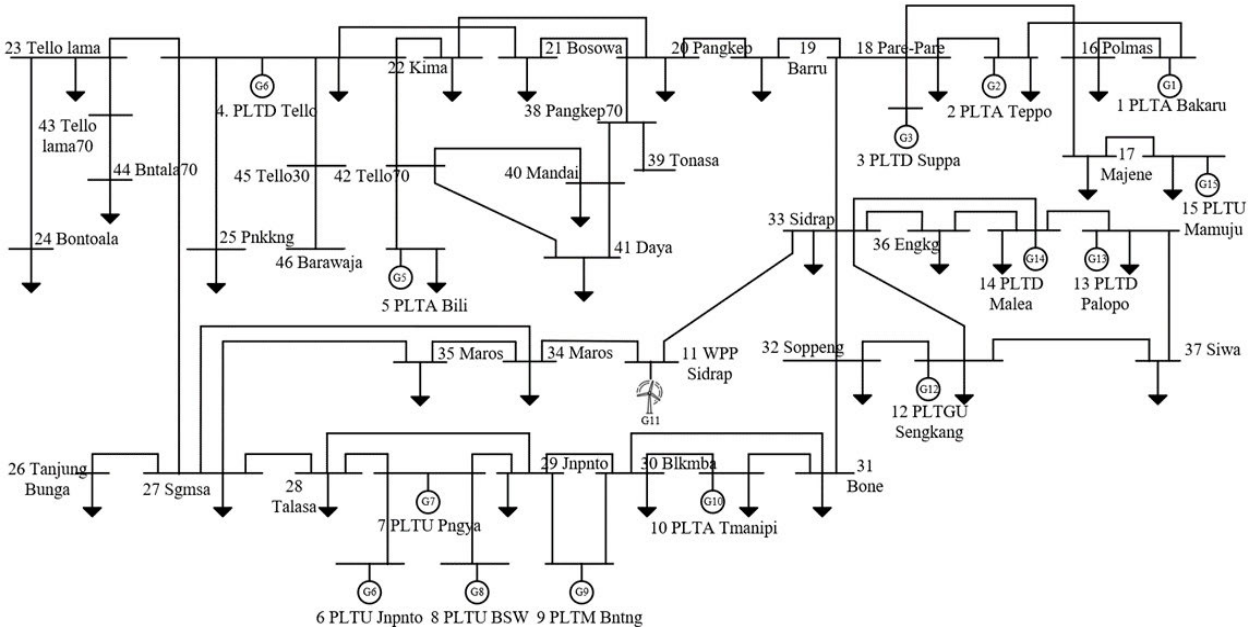

FIGURE 6. Single-line sulselrabar system with integrated WPP SIDRAP.

A. MOA ALGORITHM

This study proposes the utilization of MOA as an optimization technique. To validate the efficacy of the MOA approach, we conducted a comparative study by employing PSO and FA with the same objective function. This study sheds light on the mayfly species, known for its remarkably short twenty-four-hour life span. The researchers observed a distinction between male and female mayflies within flocks, noting that, owing to inherent strength differences, male mayflies consistently exhibit higher optimization levels than females. This characteristic bears resemblance to PSO, wherein individuals in the PSO algorithm, analogous to mayflies, update their positions $x_i(t)$ and speeds $v_i(t)$ based on their current state.

1) THE ACTIONS OF MALE MAYFLIES

Equation (6) illustrates that male mayflies adjust their position based on their individual speed in the context of the MOA. x_i is the position of the male mayfly i at the current time step t in the search space.

$$x_i(t+1) = x_i(t) + v_i(t+1) \tag{6}$$

During the iteration process described in [72], the male mayfly actively engages in both exploration and exploitation duties. In updating its speed, the mayfly takes into consideration the most recent fitness value, denoted as $f(x_i)$, and the best fitness value observed on its trajectory in the past, represented as $f(\mathrm{x_{hi}})$. Specifically, if $f(x_i)$ is greater than $f(\mathrm{x_{hi}})$, the male mayfly adjusts its speed. The modification is determined by three factors: its present speed, the separation between its current location and the world's ideal location, and the best trajectory in the past. This adaptive speed adjustment enables the male mayfly to optimize its movement strategy when it perceives an improvement in fitness. The process is mathematically represented in Equation (7).

$$v_i(t+1) = g.v_i(t) + a_i e^{-\beta r_p^2}\left[x_{hi} - x_i(t)\right] + a_2 e^{-\beta r_g^2}\left[x_g - x_i(t)\right] \tag{7}$$

The described process entails the linear descent of the variable g from its highest to lowest values, guided by weight-balancing parameters a_1, a_2, and β. The variables r_p and r_g are used to calculate the Cartesian distance between individuals and their historical best placements within the swarm. Specifically, Equation (8) is utilized to calculate the second norm for distance arrays in Cartesian space. The distances between individuals and their historically optimal locations within the swarm are quantified by Equation (8).

$$\left|\left|x_i - x_j\right|\right| = \sqrt{\sum_{k=1}^{n}\left(x_{ik} - x_{jk}\right)^2} \tag{8}$$

The male mayfly utilizes a random dance coefficient, denoted as *'d,'* to update its speed from the current value when the fitness value $f(x_i)$ is less than $f(x_{hi})$, as specified in Equation (9). Here, r_i represents a uniformly distributed random number within the domain $[-1, 1]$.

$$v_i(t+1) = g(v_i(t) + d.r_i \tag{9}$$

2) THE ACTIONS OF FEMALE MAYFLIES

Female mayflies exhibit distinct behaviors compared with male mayflies. Instead of congregating, they actively seek out males for breeding purposes. Considering that it is the current position of the female mayfly in the search space at time step t, its position can be changed by adding the velocity $v_i(t+1)$ to the current position, as shown in Equation (10):

$$y_i(t+1) = y_i(t) + v_i(t+1) \tag{10}$$

Various methods have been employed to update the speeds of female mayflies. Wingless female mayflies typically have a lifespan of one to seven days. Given this brief period, they exhibited a sense of urgency in locating male mayflies for mating and breeding. As discussed in [72], female mayflies adapt their speed in response to the characteristics and actions of the chosen male mayfly.

If $f(y_i) > f(x_i)$, the i-th female mayfly will utilize Equation (11) to update its speed. In this equation, the speed is adjusted by an additional constant, a_3, and the Cartesian distance between them is represented by r_m.

$$v_i(t+1) = g.v_i(t) + a_3 e^{-\beta r_{mf}^2} [x_i(t) - y_i(t)] \quad (11)$$

When $f(y_i) < f(x_i)$, the female mayfly adjusts its speed by employing a distinct random dance coefficient denoted as fl. As illustrated in Equation (12), the variable r_2 represents a randomly generated value selected from the range $[-1, 1]$.

$$v_i(t) = g.v_i(t) + fl.r_2 \quad (12)$$

3) MAYFLIES MATING

Each female mayfly and the majority of male mayflies participate in mating, leading to offspring production. The progeny undergo random evolutionary changes and inherit qualities from their parents, as outlined in Equations (13) and (14). In this context, L, which represent the set of random numbers, consists of random numbers generated from a Gaussian distribution.

$$offspring1 = L * male + (1 - L) * female \quad (13)$$

$$offspring2 = L * female + (1 - L) * male \quad (14)$$

4) MAYFLIES VARIATION

To address the potential issue of early convergence, wherein the optimal value may be a local optimum rather than a global one, we introduced a normally distributed random number into the mutation process for mayfly offspring. The mutation formula for mayfly offspring is represented by Equation (15):

$$offspring_n = offspring_n + \sigma.N(0, 1) \quad (15)$$

where σ is the standard deviation of the normal distribution. $N(0, 1)$ represents a standard normal distribution with a mean of zero and variance of one. The number of mutant individuals was calculated to be approximately 5% of the total number of male mayflies, rounded to the nearest whole number.

The basic structure of the MOA in carrying out the optimization process is summarized in the pseudo code shown in Table 3.

TABLE 3. Pseudo code of MOA.

Mayfly Algorithm
Determine the objective function $f(x)$, $x=(x_1, \ldots, x_d)^T$
for each male mayfly i
Initialize the male mayfly population x_i (i=1,2,...,N) & velocities v_{mi}
Evaluate male mayfly i and set $\boldsymbol{x_{hi}} = x_i$, according to Eq.(3)
end for
$\boldsymbol{x_g}$=min{$\boldsymbol{x_{hi}}$}
for each female mayfly I
Initialize the female mayfly population y_i(i=1,2,...,N) & velocities v_{fi}
Evaluate male mayfly i
end for
While stopping criteria are not met
for i=1 to N
Update velocities of males, according to Eq.(7) or Eq.(9)
Update solutions of males, according to Eq.(6)
Evaluate update solutions
end for
for i=1 to N
Update velocities of females, according to Eq.(11)
Update solutions of females, according to Eq.(10)
Evaluate updated solutions
end for
Rank the male and female mayflies
for i=1 to $N/2$
Mate the male & female mayflies, according to Eq.(13)&Eq.(14)
Evaluate offspring
end for
Separate offspring to male and female randomly
Replace worst solution with the best new ones
Update $\boldsymbol{x_{hi}}$ and $\boldsymbol{x_g}$
end while
Post process results and visualization (Best PSS parameters)

B. OBJECTIVE FUNCTION

The investigation focused on three primary aspects: the system stability, voltage improvement, and optimal power flow. This study particularly focused on optimizing the WPP size to achieve voltage improvement and optimal power flow. Simultaneously, the pursuit of optimal system stability involves optimizing the tuning and location of MB-PSS. A time-domain simulation approach was employed to assess the stability performance of the system. This facilitated the examination of various generator responses, including the rotor angle responses, output voltage response (V_{pss}), field voltage (E_{FD}), and speed deviation. Additionally, eigenvalue analysis was conducted to evaluate the efficacy of each control strategy. Using a mathematical model of the Sulselrabar system, an eigenvalue analysis was used to examine the eigenvalues of the system. Equations (16) and (17) were employed to transform the derived mathematical model into a state-space representation. The stability of the system was ascertained using Equation (18) to examine the eigenvalues of the system matrix A.

$$\Delta\dot{x} = A\Delta x + B\Delta u \quad (16)$$

$$\Delta y = C\Delta x + D\Delta u \quad (17)$$

$$\det(\text{sI-A}) = 0 \quad (18)$$

Equation (19) provides the representation of each eigenvalue (λ_i) of matrix A using complex numbers, where the real part is denoted as σ_i, and the imaginary part is represented by $j\omega_i$, with 'j' being the imaginary unit. Equation (20) defines the frequency (f) corresponding to the angular frequency (ω) of each eigenvalue.

$$\lambda_i = \sigma_i + j\omega_i \quad (19)$$

$$f = \frac{\omega}{2\pi} \quad (20)$$

The damping component is represented by the real part of the eigenvalues, and the oscillation component is represented by an imaginary part. Equation (21) provides the damping value, and Equation (22) establishes the CDI, which represent the damping of the entire system.

$$\zeta_i = \frac{-\sigma_i}{\sqrt{\sigma_i^2 + \omega_i^2}} \tag{21}$$

$$CDI = \sum_{i=1}^{n} (1 - \zeta_i) \tag{22}$$

The objective of MOA is to maximize ζ_{min}, which represents the least damping coefficient. The optimal constraints for the parameters of MB-PSS3C are specified in Equations (23)–(33), and the tuning range for the PSS parameters is detailed in Table 4.

$$K_{s1(min)} \leq K_{s1} \leq K_{s1(max)} \tag{23}$$
$$K_{s2(min)} \leq K_{s2} \leq K_{s2(max)} \tag{24}$$
$$T_{1(min)} \leq T_1 \leq T_{1(max)} \tag{25}$$
$$T_{2(min)} \leq T_2 \leq T_{2(max)} \tag{26}$$
$$T_{3(min)} \leq T_3 \leq T_{3(max)} \tag{27}$$
$$T_{4(min)} \leq T_4 \leq T_{4(max)} \tag{28}$$
$$T_{d1(min)} \leq T_{d1} \leq T_{d1(max)} \tag{29}$$
$$T_{d2(min)} \leq T_{d2} \leq T_{d2(max)} \tag{30}$$
$$T_{w1(min)} \leq T_{w1} \leq T_{w1(max)} \tag{31}$$
$$T_{w2(min)} \leq T_{w2} \leq T_{w2(max)} \tag{32}$$
$$T_{w3(min)} \leq T_{w3} \leq T_{w3(max)} \tag{33}$$

TABLE 4. Typical range for PSS parameters.

Parameter	Lower Bound (LB)	Upper Bound (U_B)
K_{s1}	0.01	200
K_{s2}	0.01	200
T_1	0.01	200
T_2	0.01	50
T_3	0.01	1
T_4	0.01	1
T_{d1}	0.01	1
T_{d2}	0.01	1
T_{w1}	0.01	1
T_{w2}	0.01	1
T_{w3}	0.01	1

The evolution of the optimization process through various strategies is depicted in the convergence graph in Fig. 7. In the 50th iteration, the PSO method attained a fitness function value of 80.53851804 and converged by the 30th iteration. Meanwhile, the FA method yielded a fitness function value of 80.49950485, which converged by the 16th iteration. In comparison, the MOA technique achieved a minimum fitness function value of 80.4372791 at the 13th iteration. These results suggest that the MOA approach outperforms the PSO and FA methods in terms of computational speed to attain a minimum fitness function value. The fitness function represents the objective function being optimized, which in this case may be related to system stability or another relevant

TABLE 5. Algorithm parameters.

Method	Parameters	Values
FA	Alpha	0.25
	Beta	0.2
	Gamma	1
	Dimension	80
	Number of Firefly	80
	Maximum Iteration	50
PSO	Particles	30
	Most Iterations	50
	The quantity of variables	8
	C2 Social Constant	2
	C1 Cognitive Constant	2
	W Moment Inersia	0.9
MOA	Population (males & females)	20
	Weight of Inertia (g)	0.8
	Ratio of Inertia for Damping Weight (a_1)	1
	Coefficient of Global Learning (a_2, a_3)	1.5
	Sight Coefficient for Distance (β)	2
	The Wedding Dance	5
	Random flight (f1)	1
	Damping Ratio (dance_damp)	0.8
	Parameters for Mating (fl_damp)	0.99
	Total Offspring Count (nc)	20
	Total Mutant Count	(0.05*nPop)
	Rate of Mutation (mu)	0.01

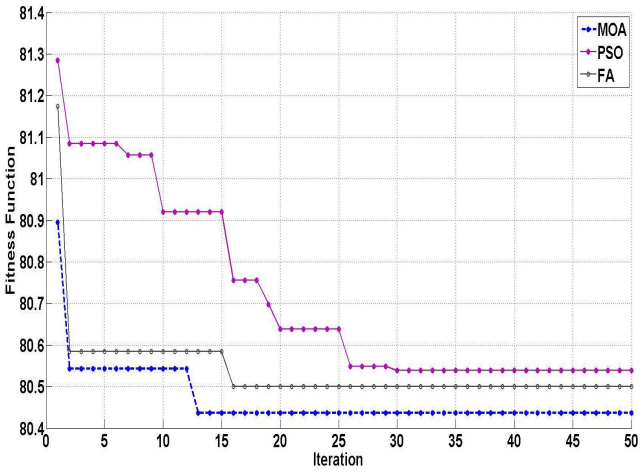

FIGURE 7. Convergence graphic.

metric. The method parameters initialized in this study are listed in Table 5. The MOA algorithm integrates features from both PSO and FA [33], thereby enhancing global search efficiency. As a hybrid optimization algorithm, the MOA models the mating patterns of mayflies, resulting in a high-efficiency optimization. Fig. 8 illustrates the system modeling design using the Simulink Model.

Fig. 9 shows the optimization procedure for the MB-PSS3C parameter placement and adjustment. The research began with data collection using the Sulselrabar system. The next stage involves system modeling, initializing the PSS parameters, and determining the objective function. Subsequently, an initial load flow study with a WPP injection was conducted. Once the load flow data were obtained, they were utilized to optimize the PSS parameters using the MOA algorithm. This algorithm operates based on an objective

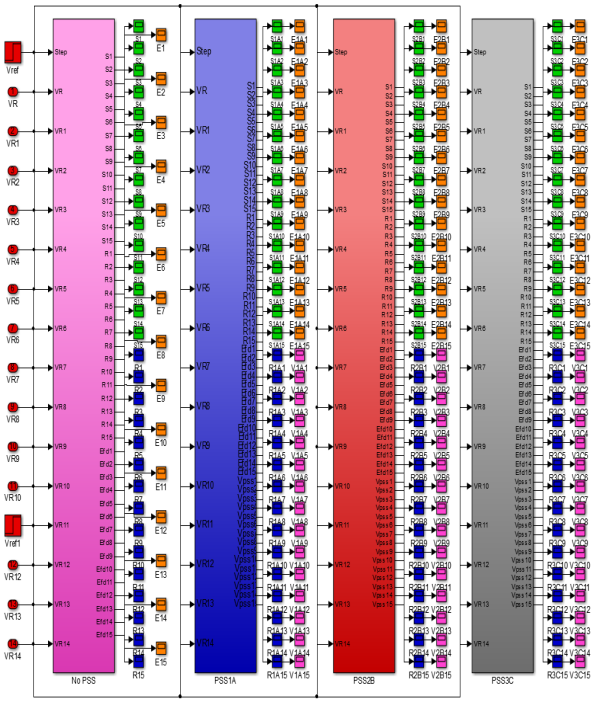

FIGURE 8. System model.

function aimed at maximizing the damping and eigenvalues of the system. The PSS placement option was selected based on the maximum damping and the optimal eigenvalue.

The objective function focuses on maximizing the minimum damping (ζ_{min}) in the system, where ζ_{min} represents the minimum level of damping achieved. After determining the optimal PSS placement, the response of the system was monitored and analyzed. For each generator, this involves evaluating the rotor angle response, PSS Voltage Output Response (V_{pss}), Field Voltage Response (E_{fd}), and Speed Deviation ($\Delta\omega$). The study also encompasses an investigation of the overshoot and eigenvalues of each generator. The linear model of the system is subjected to disturbance input, specifically modifications in the 0.5 pu load requirements applied to the WPP SIDRAP and BAKARU generators. The generator's angular speed response (ω) decreases as a result of an increase in the load demand, which causes the incoming mechanical power (P_m) to become less than the departing electrical power (P_e).

IV. RESULTS AND DISCUSSION

This section presents the results of the discussion on load flow, emphasizing the application of MB-PSS3C with damping system analysis, time-domain simulation, and eigenvalue analysis. The findings and insights gained from these analyses contribute to a comprehensive understanding of the behavior and performance of a system under various conditions.

A. LOAD FLOW RESULTS

The analysis begins with load flow calculations aimed at evaluating the voltage profile and power flow in the Sulselrabar system, both before and after power injection from the WPP. The results of these calculations, which were conducted using the Newton-Raphson method, are presented in Table 6. It is noteworthy that this research adopts the latest transmission configuration, which includes 15 generators, 57 transmission lines, and 46 buses. To enhance the system performance, shunt capacitors are strategically placed on specific buses, including buses 30 BULUKUMBA and 31 BONE (30 MVar), bus 38 PANGKEP (50 MVar), bus 41 DAYA (20 MVar), as well as buses 42 TELLO and 43 TELLO LAMA (10 MVar).

Table 6 presents a comparison of the power flow parameters before and after the injection of 31 MW power from the WPP SIDRAP. The simulation results revealed that the inclusion of the WPP SIDRAP leads to a more optimal power flow and smaller losses. Before the WPP SIDRAP injection, the Active Power was 56.361 MW, and Reactive Power was 238.599 MVar. After the injection, the Reactive Power loss decreased to 231.080 MVar, and Active Power loss dropped to 54.626 MW. These findings highlight the positive impact of WPP SIDRAP on the line flow characteristics and overall system losses.

Moreover, the injection of WPP SIDRAP improved the voltage profile of the Sulselrabar system, as illustrated in Fig. 10. Prior to the injection, several buses experienced marginal and critical voltage conditions. According to system operating guidelines, the minimum bus voltage should not fall below 5% of the nominal voltage. As shown in Fig. 10, marginal voltage conditions occurred on buses 25, 26, 27, and 28, with a voltage range of 0.95 pu to 0.97 pu, while critical voltage conditions occurred on bus 46 with a voltage $<$ 0.95 pu. Following injection from the WPP SIDRAP, there was a notable improvement in the voltage profile of the bus.

B. MB-PSS3C OPTIMIZATION

After achieving optimal line flow and minimizing losses through the integration of the WPP SIDRAP on bus 11, an analysis was conducted to enhance the stability of the Sulselrabar system. In this study, a load change scenario was introduced at the BAKARU bus and WPP SIDRAP to evaluate the performance of each generator. MATLAB SIMULINK was used for system modeling, while MATLAB M-files were employed for data processing and implementation of the MOA algorithms. The analysis of voltage magnitudes was based on load flow studies conducted after the incorporation of the WPP SIDRAP into the Sulselrabar system. Subsequently, a matrix for network reduction was created, and the outcomes were used to simulate the system. The simulation encompassed several models, including SB-PSS1A, MB-PSS2B, MB-PSS3C, and systems without PSS. The eigenvalues of the system were investigated through PSS simulations to provide insights into its stability. The primary goal was to observe the increased damping, indicating improved stability. The analysis of system eigenvalues in simulations without PSS aimed to reveal an augmentation

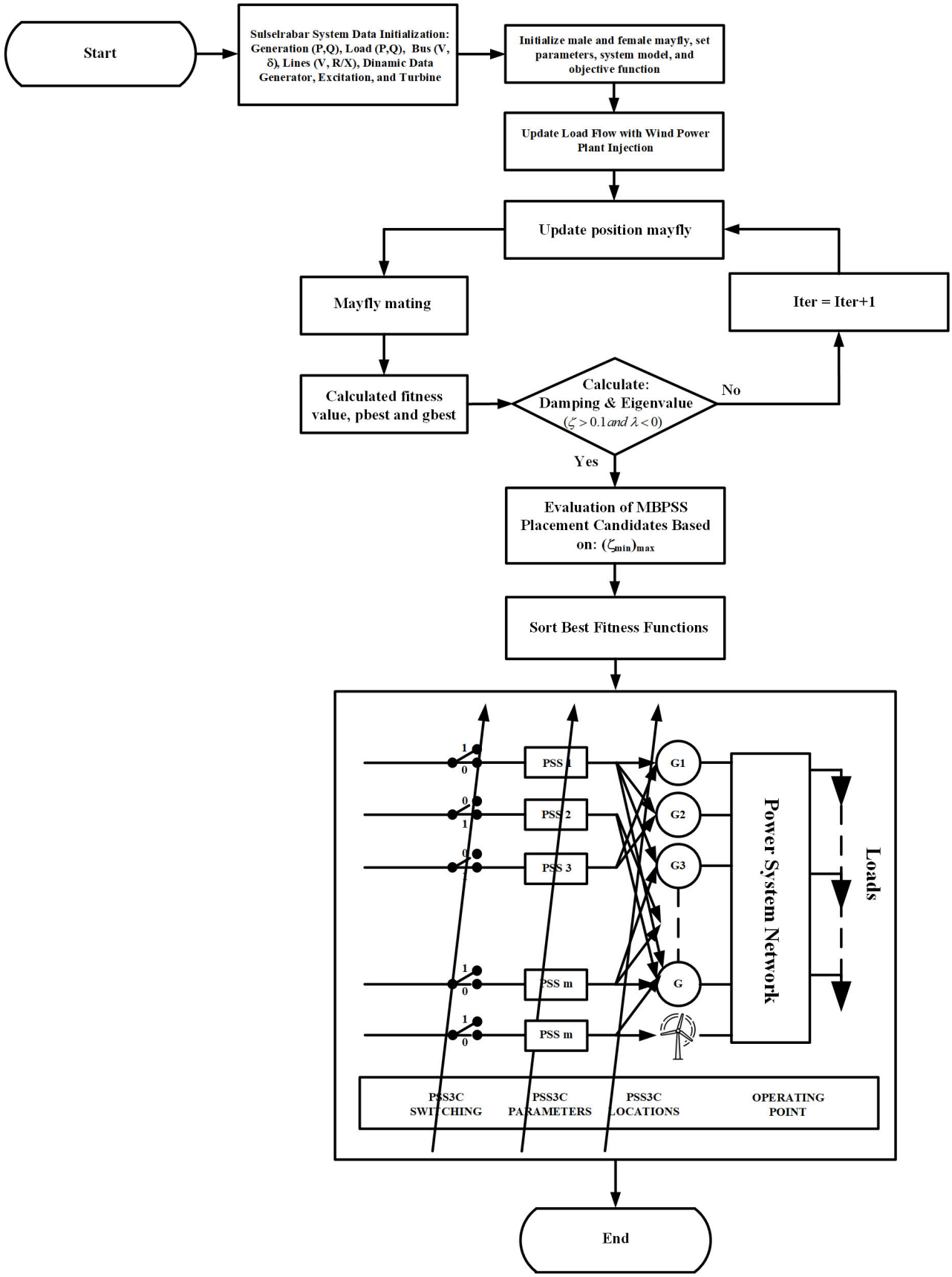

FIGURE 9. Flowchart of research procedures.

TABLE 6. Load flow analysis results for the sulselrabar system.

Line		Line Flow and Losses Before Injection WPP				Line Flow and Losses After Injection WPP			
From	To	Line Flow		Losses		Line Flow		Losses	
		P(MW)	Q(MVar)	P(MW)	Q(MVar)	P(MW)	Q(MVar)	P(MW)	Q(MVar)
1	16	34.246	48.395	0.782	1.093	20.366	51.672	0.690	0.762
	2	50.815	84.747	2.535	6.849	31.660	89.752	2.359	6.217
2	1	-48.279	-77.898	2.535	6.849	-29.301	-83.535	2.359	6.217
	18	19.579	-10.173	0.066	-1.107	0.601	-6.173	0.004	-1.328
3	18	40.000	-18.234	0.152	0.433	40.000	-20.294	0.158	0.456
	23	82.636	14.154	0.510	1.654	82.636	14.154	0.510	1.654
	27	-264.312	147.089	3.524	23.877	-279.114	150.389	3.872	26.255
	21	-7.924	0.011	0.011	-1.485	1.158	-4.227	0.002	-1.517
4	25	73.105	20.889	2.505	4.589	73.105	20.889	2.505	4.589
	45	35.573	1.017	0.307	-1.210	35.573	1.017	0.307	-1.210
	42	35.026	-14.286	0.338	-1.130	35.802	-14.665	0.354	-1.074
	22	-3.704	0.570	0.004	-2.318	1.240	-1.747	0.000	-2.333
5	42	10.500	-8.729	0.113	0.139	10.500	-8.877	0.114	0.142
6	7	190.000	-25.619	0.647	3.986	190.000	-25.619	0.647	3.986
	28	416.557	55.665	9.064	60.803	412.080	54.347	415.648	8.866
7	6	-189.353	29.605	0.647	3.986	-189.353	29.605	191.654	0.647
	8	-229.099	68.374	2.401	8.379	-229.099	68.374	239.084	2.401
	29	87.895	-17.876	1.452	4.197	92.372	-18.576	94.221	1.603
8	7	231.500	-59.995	2.401	8.379	231.500	-59.995	2.401	8.379
9	29	-49.898	15.053	0.140	-0.361	-53.016	16.044	0.159	-0.236
	30	40.598	-26.198	0.118	-0.527	43.716	-26.571	0.132	-0.428
10	30	-32.766	2.617	0.339	-0.559	-35.546	3.520	0.400	-0.338
	31	15.966	-17.935	0.218	-1.557	18.746	-18.462	0.265	-1.389
11	34	38.794	27.669	0.161	0.701	58.040	25.363	0.284	1.442
	33	-38.794	9.067	1.010	3.680	-26.740	5.207	0.474	0.453
	32	30.994	-8.341	0.216	0.485	29.018	-8.017	0.190	0.329
12	33	87.494	-7.844	1.624	8.963	89.126	-8.516	1.687	9.341
	37	43.012	-9.370	0.655	0.430	43.356	-9.419	0.665	0.467
13	14	-1.071	0.022	0.000	-0.552	-0.750	-0.068	0.000	-0.553
	37	-33.529	10.663	0.629	-0.537	-33.850	10.794	0.641	-0.492
	33	-1.781	-0.200	0.003	-2.384	-1.669	-0.420	0.002	-2.389
14	36	-3.191	2.491	0.007	-0.527	-2.982	1.945	0.005	-0.533
	13	1.072	-0.574	0.000	-0.552	0.751	-0.485	0.000	-0.553
15	17	13.900	-14.329	0.204	-0.025	13.900	-14.425	0.206	-0.020
	1	-33.464	-47.302	0.782	1.093	-19.676	-50.910	0.690	0.762
16	18	25.531	29.033	0.537	-1.902	11.741	32.535	0.442	-2.246
	17	1.133	15.969	0.129	-0.334	1.136	16.076	0.130	-0.329
17	16	-1.004	-16.303	0.129	-0.334	-1.006	-16.404	0.130	-0.329
	15	-13.696	14.303	0.204	-0.025	-13.694	14.404	0.206	-0.020
	2	-19.514	9.066	0.066	-1.107	-0.597	4.844	0.004	-1.328
	3	-39.848	18.667	0.152	0.433	-39.842	20.750	0.158	0.456
18	19	111.645	-22.000	2.973	8.418	95.132	-21.029	2.174	5.550
	16	-24.994	-30.935	0.537	-1.902	-11.298	-34.781	0.442	-2.246
	33	-46.689	20.401	0.519	1.581	-62.795	25.416	0.916	3.007
19	18	-108.672	30.417	2.973	8.418	-92.957	26.580	2.174	5.550
	20	106.072	-30.917	2.946	8.217	90.357	-27.080	2.135	5.302
	19	-103.126	39.134	2.946	8.217	-88.223	32.381	2.135	5.302
20	21	39.246	-1.275	0.111	0.221	30.111	2.769	0.066	0.058
	22	16.361	0.919	0.053	-0.093	11.388	3.129	0.028	-0.185
	38	22.019	-47.078	0.287	0.025	21.224	-46.579	0.278	-0.012
21	4	7.934	-1.496	0.011	-1.485	-1.155	2.710	0.002	-1.517
	20	-39.134	1.496	0.111	0.221	-30.045	-2.710	0.066	0.058
22	4	3.708	-2.889	0.004	-2.318	-1.240	-0.586	0.000	-2.333
	20	-16.308	-1.011	0.053	-0.093	-11.360	-3.314	0.028	-0.185
	4	-82.125	-12.500	0.510	1.654	-82.125	-12.500	0.510	1.654
23	43	5.031	-8.600	0.020	-0.209	5.031	-8.600	0.020	-0.209
	24	34.794	9.500	0.094	0.300	34.794	9.500	0.094	0.300
24	23	-34.700	-9.200	0.094	0.300	-34.700	-9.200	35.899	0.094
25	4	-70.600	-16.300	2.505	4.589	-70.600	-16.300	2.505	4.589
26	27	-56.600	-15.800	0.263	1.328	-56.600	-15.800	0.263	1.328
	4	267.836	-123.212	3.524	23.877	282.985	-124.133	3.872	26.255
	26	56.863	17.128	0.263	1.328	56.863	17.128	0.263	1.328
27	28	-369.319	114.039	15.273	104.101	-365.392	111.588	14.921	101.687
	34	-5.732	-12.465	0.023	-0.607	-17.317	-10.393	0.052	-0.409
	35	2.352	-6.990	0.006	-0.718	-5.139	-5.689	0.007	-0.713
28	27	384.592	-9.938	15.273	104.101	380.313	-9.901	14.921	101.687
	7	-407.492	5.138	9.064	60.803	-403.213	5.101	8.866	59.448

TABLE 6. *(Continued.)* **Load flow analysis results for the sulselrabar system.**

	7	-86.443	22.073	1.452	4.197	-90.769	23.313	1.603	4.738
29	30	16.704	-10.260	0.184	-0.028	17.895	-10.633	0.208	0.058
	9	50.039	-15.414	0.140	-0.361	53.174	-16.280	0.159	-0.236
	29	-16.520	10.232	0.184	-0.028	-17.687	10.691	0.208	0.058
30	9	-40.480	25.671	0.118	-0.527	-43.583	26.143	0.132	-0.428
	10	33.105	-3.176	0.339	-0.559	35.947	-3.858	0.400	-0.338
	31	11.895	-6.127	0.238	-1.232	13.323	-6.376	0.292	-1.035
	30	-11.658	4.894	0.238	-1.232	-13.031	5.341	0.292	-1.035
31	10	-15.748	16.378	0.218	-1.557	-18.482	17.073	0.265	-1.389
	32	12.706	4.927	0.084	-0.524	16.813	3.786	0.133	-0.350
	31	-12.622	-5.451	0.084	-0.524	-16.680	-4.136	0.133	-0.350
32	12	-30.778	8.826	0.216	0.485	-28.829	8.346	0.190	0.329
	33	34.300	-5.275	0.671	1.445	36.409	-6.110	0.759	1.762
	18	47.208	-18.820	0.519	1.581	63.710	-22.409	0.916	3.007
	32	-33.629	6.720	0.671	1.445	-35.649	7.872	0.759	1.762
33	12	-85.870	16.807	1.624	8.963	-87.439	17.857	1.687	9.341
	14	1.784	-2.184	0.003	-2.384	1.671	-1.969	0.002	-2.389
	36	10.903	-3.235	0.005	-0.217	10.693	-2.697	0.005	-0.219
	11	39.805	-5.387	1.010	3.680	27.215	-4.754	0.474	0.453
	27	5.755	11.859	0.023	-0.607	17.369	9.984	0.052	-0.409
34	11	-38.633	-26.968	0.161	0.701	-57.756	-23.920	0.284	1.442
	35	14.978	10.009	0.023	-0.263	22.487	8.836	0.041	-0.140
35	27	-2.345	6.272	0.006	-0.718	5.146	4.976	0.007	-0.713
	34	-14.955	-10.272	0.023	-0.263	-22.446	-8.976	0.041	-0.140
36	33	-10.898	3.018	0.005	-0.217	-10.687	2.478	0.005	-0.219
	14	3.198	-3.018	0.007	-0.527	2.987	-2.478	0.005	-0.533
37	13	34.158	-11.200	0.629	-0.537	34.491	-11.286	0.641	-0.492
	12	-42.358	9.800	0.655	0.430	-42.691	9.886	0.665	0.467
	20	-21.732	47.103	0.287	0.025	-20.946	46.567	0.278	-0.012
38	39	0.000	-0.010	0.000	-0.010	0.000	-0.010	0.000	-0.010
	40	7.732	-0.492	0.210	0.283	6.946	0.044	0.168	0.207
39	38	0.000	0.000	0.000	-0.010	0.000	-0.000	0.000	-0.010
	38	-7.522	0.776	0.210	0.283	-6.778	0.164	0.168	0.207
40	41	-5.412	-5.407	0.020	-0.001	-5.785	-5.103	0.020	-0.000
	42	-15.266	1.432	0.138	0.190	-15.637	1.740	0.145	0.203
41	40	5.432	5.407	0.020	-0.001	5.805	5.103	0.020	-0.000
	42	-29.432	11.193	0.238	0.411	-29.805	11.497	0.245	0.424
	4	-34.687	13.157	0.338	-1.130	-35.448	13.591	0.354	-1.074
42	40	15.404	-1.242	0.138	0.190	15.783	-1.537	0.145	0.203
	41	29.670	-10.782	0.238	0.411	30.051	-11.073	0.245	0.424
	5	-10.387	8.868	0.113	0.139	-10.386	9.019	0.114	0.142
43	23	-5.011	8.391	0.020	-0.209	-5.011	8.391	0.020	-0.209
	44	5.011	1.609	0.011	0.009	5.011	1.609	0.011	0.009
44	43	-5.000	-1.600	0.011	0.009	-5.000	-1.600	0.011	0.009
45	4	-35.266	-2.227	0.307	-1.210	-35.266	-2.227	0.307	-1.210
	46	35.266	2.227	1.566	2.227	35.266	2.227	1.566	2.227
46	45	-33.700	0.000	1.566	2.227	-33.700	0.000	1.566	2.227
Total				**56.361**	**238.599**			**54.626**	**231.080**

in damping, contributing to the enhanced stability of the Sulselrabar system.

The results of MB-PSS3C parameter tuning are provided in Tables 7-9, detailing the specific parameter values obtained through the PSO, FA, and MOA-based tuning methods. Additionally, the tuning results from previous research [33] were utilized for the MB-PSS1A and MB-PSS2B parameters. The PSS placement index was assessed using the MOA as the proposed method. The highest value of ζ_{min}, considered more relevant than ζ_0 (which may represent initial damping), was considered when determining the priority for PSS placement. A comparison of the priority location placement indices intended for the PSS installation is shown in Fig. 11. This graph illustrates the influence of the minimal damping eigensystem of each installation plan on the occupancy index at each location. After the addition of the PSS, the system damping value increased. The MB-PSS3C based control scheme with 14 PSS placement options exhibited superior damping compared to the other control schemes. In this study, the proposed control scheme based on MB-PSS3C-MOA achieved a maximum damping value of 0.7498925, while MB-PSS3C-PSO damping was 0.722003831, and MB-PSS3C-FA damping was 0.733272031. A system is considered to have good damping if the value exceeds 0.1, indicating the stability and effective damping of the oscillations.

1) TIME DOMAIN SIMULATION

This section specifically addresses the system stability of Bus 1, associated with the BAKARU generator, and Bus 11, corresponding to WPP SIDRAP. The BAKARU generator, with an impressive installed power capacity of 126 MW,

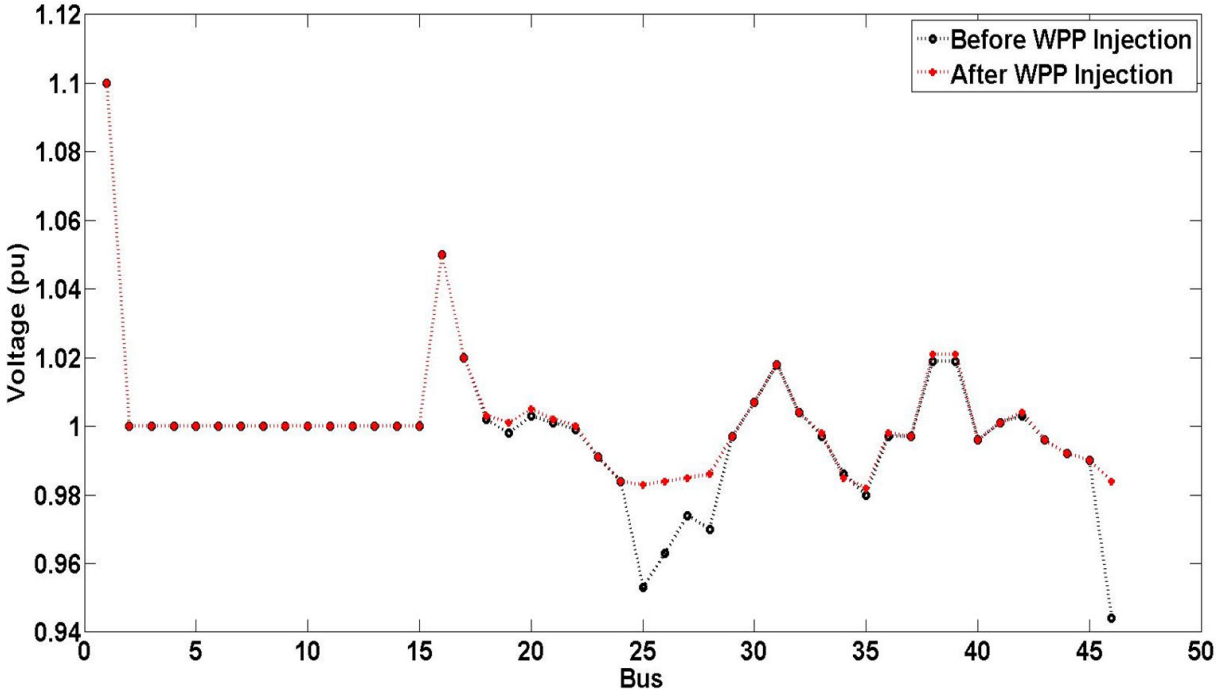

FIGURE 10. Voltage profile comparison.

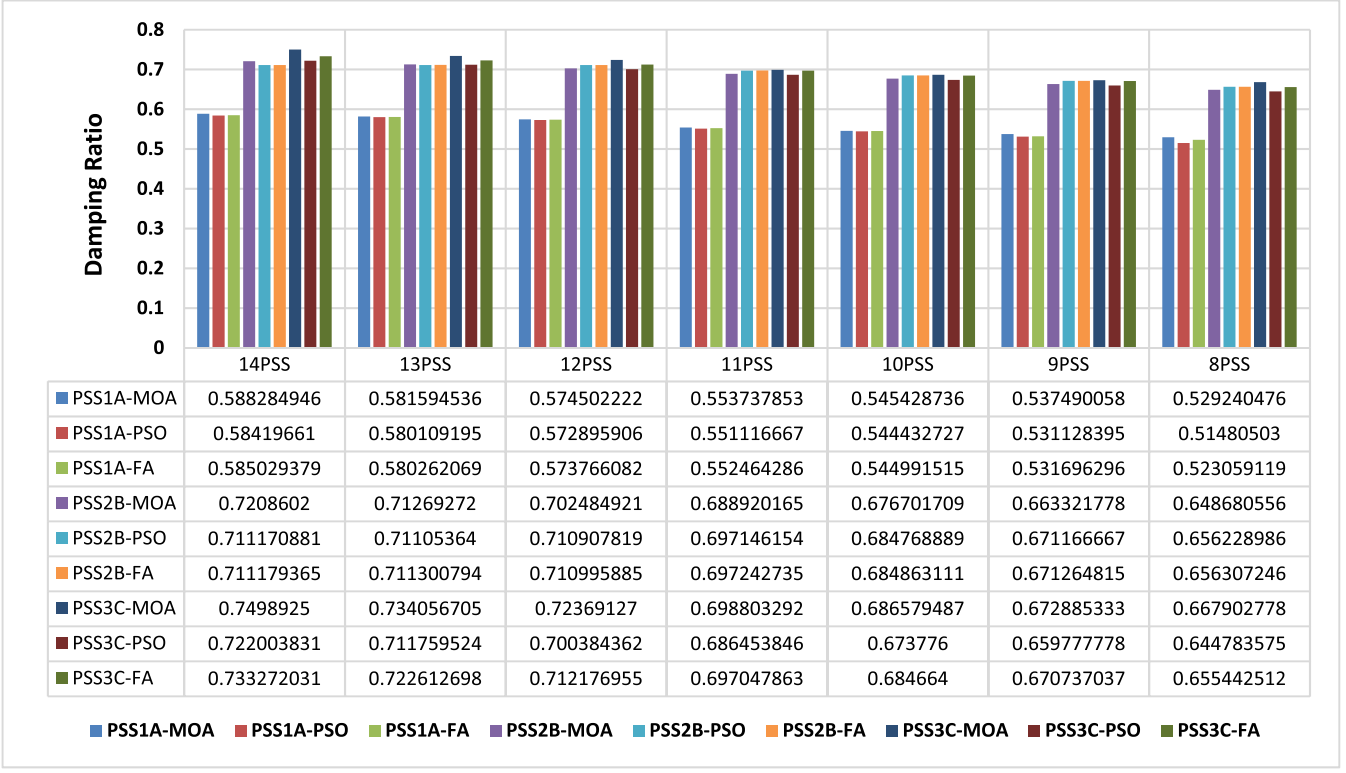

	14PSS	13PSS	12PSS	11PSS	10PSS	9PSS	8PSS
PSS1A-MOA	0.588284946	0.581594536	0.574502222	0.553737853	0.545428736	0.537490058	0.529240476
PSS1A-PSO	0.58419661	0.580109195	0.572895906	0.551116667	0.544432727	0.531128395	0.51480503
PSS1A-FA	0.585029379	0.580262069	0.573766082	0.552464286	0.544991515	0.531696296	0.523059119
PSS2B-MOA	0.7208602	0.71269272	0.702484921	0.688920165	0.676701709	0.663321778	0.648680556
PSS2B-PSO	0.711170881	0.71105364	0.710907819	0.697146154	0.684768889	0.671166667	0.656228986
PSS2B-FA	0.711179365	0.711300794	0.710995885	0.697242735	0.684863111	0.671264815	0.656307246
PSS3C-MOA	0.7498925	0.734056705	0.72369127	0.698803292	0.686579487	0.672885333	0.667902778
PSS3C-PSO	0.722003831	0.711759524	0.700384362	0.686453846	0.673776	0.659777778	0.644783575
PSS3C-FA	0.733272031	0.722612698	0.712176955	0.697047863	0.684664	0.670737037	0.655442512

FIGURE 11. Placement index damping system.

is one of the largest generators in the Sulselrabar system and serves as the swing generator of the system owing to its capacity and adaptability. In contrast, the WPP SIDRAP generator operates as a wind power plant in the Sulselrabar system, boasting an installed electrical capacity of 75 MW. Figs. 12 and 13 show the speed responses of both the

TABLE 7. Tuning results of MB-PSS3C parameter using PSO.

G	$K_{s1,}$	K_{s2}	T_1	T_2	T_3	T_4	T_{d1}	T_{d2}	T_{w1}	T_{w2}	T_{w3}
1	200	131.1887	80.7941	19.4635	0.2965	0.2077	0.1537	0.4560	0.2077	0.2965	0.6
2	144.3298	92.8662	120.1323	28.0100	0.2671	1.0114	0.1000	1.5000	1.0114	0.2671	0.6
3	96.9599	121.7420	98.3755	27.6264	0.2088	1.2919	0.4450	0.0733	1.2919	0.2088	0.6
4	96.3324	140.6859	90.0106	29.5484	0.1000	1.3544	0.1541	1.2499	1.3544	0.1000	0.6
5	186.1574	98.6309	92.3590	20.1914	0.4090	0.5724	0.3701	0.0137	0.5724	0.4090	0.6
6	50	124.6355	94.7207	15.2203	0.3382	0.8920	0.1000	1.5000	0.8920	0.3382	0.6
7	187.5483	101.8899	131.2151	10	0.3655	0.6191	0.4044	0.1672	0.6191	0.3655	0.6
8	50	109.4712	119.8929	20.9326	0.1000	0.1746	0.4273	0.1340	0.1746	0.1000	0.6
9	50	114.8911	150	22.0052	0.4991	1.0617	0.5000	0.1203	1.0617	0.4991	0.6
10	183.5200	124.1909	100.0521	10	0.1510	1.4051	0.2373	0.3109	1.4051	0.1510	0.6
11	194.4455	95.8206	86.5610	18.5005	0.3026	1.2664	0.4180	1.5000	1.2664	0.3026	0.6
12	200	108.6379	112.9094	10	0.1034	0.2576	0.4558	0.5652	0.2576	0.1034	0.6
13	99.0467	146.0433	100.3773	30	0.3827	0.0100	0.5000	0.2196	0.0100	0.3827	0.6
14	95.9179	95.7305	79.7364	30	0.1000	1.5000	0.2899	1.1459	1.5000	0.1000	0.6

TABLE 8. Tuning results of MB-PSS3C parameter using FA.

G	$K_{s1,}$	K_{s2}	T_1	T_2	T_3	T_4	T_{d1}	T_{d2}	T_{w1}	T_{w2}	T_{w3}
1	130.8984	104.0020	149.3131	23.9425	0.1537	0.4560	0.1537	0.4560	0.2077	0.2965	0.6
2	71.9092	85.8921	83.2407	23.9811	0.1000	1.5000	0.1000	1.5000	1.0114	0.2671	0.6
3	198.1075	91.4976	112.4068	21.7103	0.4450	0.0733	0.4450	0.0733	1.2919	0.2088	0.6
4	149.0982	136.3656	136.8930	24.3752	0.1541	1.2499	0.1541	1.2499	1.3544	0.1000	0.6
5	89.7007	127.7720	114.0791	16.6934	0.3701	0.0137	0.3701	0.0137	0.5724	0.4090	0.6
6	80.4897	102.6720	91.5512	10	0.1000	1.5000	0.1000	1.5000	0.8920	0.3382	0.6
7	130.7867	129.7630	123.0278	13.5990	0.4044	0.1672	0.4044	0.1672	0.6191	0.3655	0.6
8	160.8221	97.0642	110.1200	28.2587	0.4273	0.1340	0.4273	0.1340	0.1746	0.1000	0.6
9	154.9948	147.9914	124.2046	11.9664	0.5000	0.1203	0.5000	0.1203	1.0617	0.4991	0.6
10	61.1169	120.9374	75	25.0610	0.2373	0.3109	0.2373	0.3109	1.4051	0.1510	0.6
11	195.2379	104.9571	118.2256	17.8549	0.4180	1.5000	0.4180	1.5000	1.2664	0.3026	0.6
12	127.2711	118.4971	77.1489	15.8820	0.4558	0.5652	0.4558	0.5652	0.2576	0.1034	0.6
13	139.3321	132.7416	133.3512	13.4115	0.5000	0.2196	0.5000	0.2196	0.0100	0.3827	0.6
14	177.1889	102.5853	135.9405	25.1407	0.2899	1.1459	0.2899	1.1459	1.5000	0.1000	0.6

TABLE 9. Tuning results of MB-PSS3C parameter using MOA.

G	$K_{s1,}$	K_{s2}	T_1	T_2	T_3	T_4	T_{d1}	T_{d2}	T_{w1}	T_{w2}	T_{w3}
1	180.3052	121.0086	129.7433	12.6008	0.2852	0.3748	0.1537	0.4560	0.2077	0.2965	0.6
2	182.3955	174.2710	133.0830	17.8804	0.4482	0.7404	0.1000	1.5000	1.0114	0.2671	0.6
3	120.6458	50.2160	92.6037	17.1694	0.2366	1.4039	0.4450	0.0733	1.2919	0.2088	0.6
4	54.0775	160.9996	93.5443	12.0359	0.1249	1.3811	0.1541	1.2499	1.3544	0.1000	0.6
5	56.3847	128.5759	93.9640	13.8893	0.1132	0.2105	0.3701	0.0137	0.5724	0.4090	0.6
6	126.2464	50	104.5966	25.9079	0.1766	1.1486	0.1000	1.5000	0.8920	0.3382	0.6
7	193.8797	159.2267	132.9912	26.2650	0.3375	0.3462	0.4044	0.1672	0.6191	0.3655	0.6
8	188.1082	135.4213	122.3479	11.3309	0.3910	0.6251	0.4273	0.1340	0.1746	0.1000	0.6
9	108.8858	154.0118	141.0343	16.0456	0.4980	0.5949	0.5000	0.1203	1.0617	0.4991	0.6
10	158.3743	200	114.8044	12.4885	0.3226	0.5052	0.2373	0.3109	1.4051	0.1510	0.6
11	88.0466	50	123.2257	27.0034	0.4467	0.9885	0.4180	1.5000	1.2664	0.3026	0.6
12	191.5571	181.5008	88.2664	10.2510	0.4886	0.2488	0.4558	0.5652	0.2576	0.1034	0.6
13	178.4384	163.9626	112.3182	11.5069	0.1995	0.9517	0.5000	0.2196	0.0100	0.3827	0.6
14	173.9368	200	147.3589	22.3845	0.2509	0.2714	0.2899	1.1459	1.5000	0.1000	0.6

BAKARU and WPP SIDRAP generators in the event of a disturbance occurring on Buses 1 and 11. The speed responses of the other generators are shown in Fig. 14. These charts graphically depict the impact of disturbances on each generator's associated bus speed, offering insights into the dynamic behavior of the system during interruptions.

When subjected to load changes, the generator initially experiences a slowdown (ω), causing mechanical power (P_m) to fall short of the electrical power (P_e), creating a power imbalance. To mitigate this impact and maintain stability under such conditions, the role of the control equipment becomes pivotal. Control systems are essential for regulating the response of the generator to ensure a stable operation. As shown in Fig. 12, the performance of the exciter may be limited without additional control mechanisms, leading to fluctuating speed responses. These oscillations, ranging from −0.01953 pu to 0.004698 pu, underscore the importance of effective control systems in maintaining stability during load changes. The implementation of PSS1A control resulted in an enhancement, with a decreased overshoot within the range of −0.01629 pu to 0.002019 pu. The introduction of PSS2B resulted in oscillations ranging from −0.01183 pu

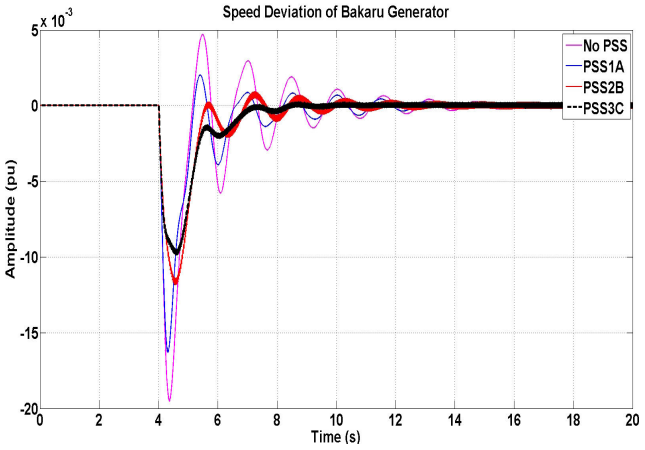

FIGURE 12. Comparison of $\Delta\omega$ response in bakaru generator.

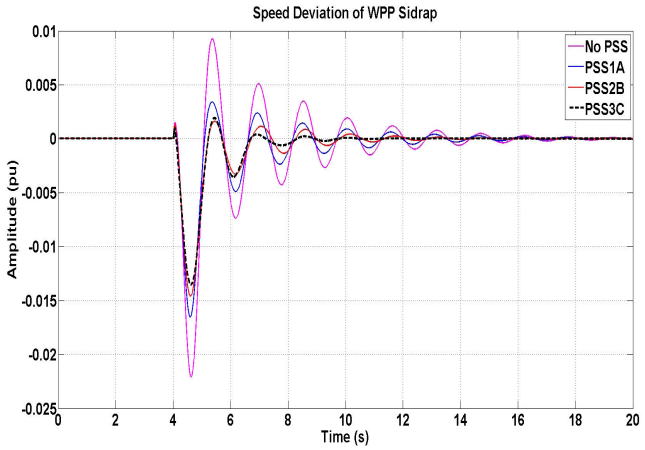

FIGURE 13. Comparison of $\Delta\omega$ response in WPP generator.

to 0.0009272 pu. The system demonstrated optimal performance when integrated with PSS3C, showing a narrow oscillation range of −0.009859 pu to 0.0002462 pu. Similarly, the response of the WPP SIDRAP generator is depicted in Fig. 13. Without additional control, the system exhibited an overrun in the range of −0.02209 pu to 0.009257 pu. The overshoot was reduced to a range of −0.01652 pu to 0.003408 pu with the introduction of PSS1A. The inclusion of PSS2B resulted in oscillations ranging from −0.01459 pu to 0.001624 pu. The application of PSS3C further improved the performance, resulting in an ideal overshoot range of −0.01354 pu to 0.001937 pu. A detailed breakdown of the speed deviations of each generator is presented in Table 10.

A detailed comparison of the speed response in the Sulselrabar generator system during a disturbance, specifically a load shift on buses 1 and 11, is provided in Table 10. The table highlights the minimum overshoot deviation observed under various control schemes, with particular emphasis on the superior performance achieved by the PSS3C-based control scheme optimized through the MOA approach. This underscores the effectiveness of additional PSS control in enhancing the response of the generator to disturbances. The enhanced control signals from the PSS, which are particularly beneficial for adjusting the generator field voltage, significantly improved the overall generator performance.

The integration of a PSS aims to optimize the control signals and enhance the field voltage response, thereby improving the behavior of the generator during disruptions. Figs. 15 and 16 show the responses of the WPP generator field voltage and BAKARU generator field voltage to a disturbance. These statistics demonstrate the superior performance of the MOA method in enhancing the system stability and control by visualizing each generator's field voltage response. Fig. 18 expands on this analysis by displaying the field voltage responses of the additional generators in the system during disturbances. This visual depiction allows us to obtain values or metrics related to parameters, such as overshoot, damping, or other relevant factors. This provides specific insights into how the field voltage of each generator responds under particular conditions.

The performance of a PSS can also be assessed by examining its output voltage response to excitation. This voltage signifies the additional signal provided by the PSS to the exciter of the generator, offering extra damping when the exciter performance is at its peak. In Fig. 17, a comparison of the PSS output voltage performance for the WPP SIDRAP generator is shown, showing the performance of various PSS types. Notably, the control scheme with PSS3C exhibited a superior response, evident from its higher voltage output compare to PSS1A and PSS2B. For a comprehensive overview of the PSS output voltage response, refer to Fig. 19.

The assessment of generator stability performance involves analyzing the rotor-angle responses. Figs. 20 and 21 illustrate the rotor angle deviation responses to disturbances at buses 1 and 11 for the WPP SIDRAP and BAKARU generator rotors, respectively. These figures offer valuable insights into the impact of disturbances on the rotor angles. Fig. 22 illustrates how the rotor angles of the additional generators in the system react to the same disturbances. This comparative analysis provides a comprehensive understanding of the impact of disturbances on the rotor angles across various system generators. Differentiating the rotor angle responses offers a clear understanding of how additional parameters affect generator oscillations and settling time. Generators without supplementary controls often exhibit significant oscillations and prolonged settling times when subjected to disturbances. This underscores the importance of incorporating supplementary controls, such as PSS, to enhance generator stability and response.

Without additional control, the settling time of the BAKARU generator in Fig. 20 was 17.74 seconds. The introduction of PSS1A improves the settling time to 13.6 seconds, further reduced to 10.75 seconds with PSS2B, and ultimately to 8.454 seconds with PSS3C. This demonstrates a gradual reduction in the settling time with the incorporation of PSS, which is notably prominent with PSS3C. Similarly, in Fig. 21, the settling time of the WPP SIDRAP generator

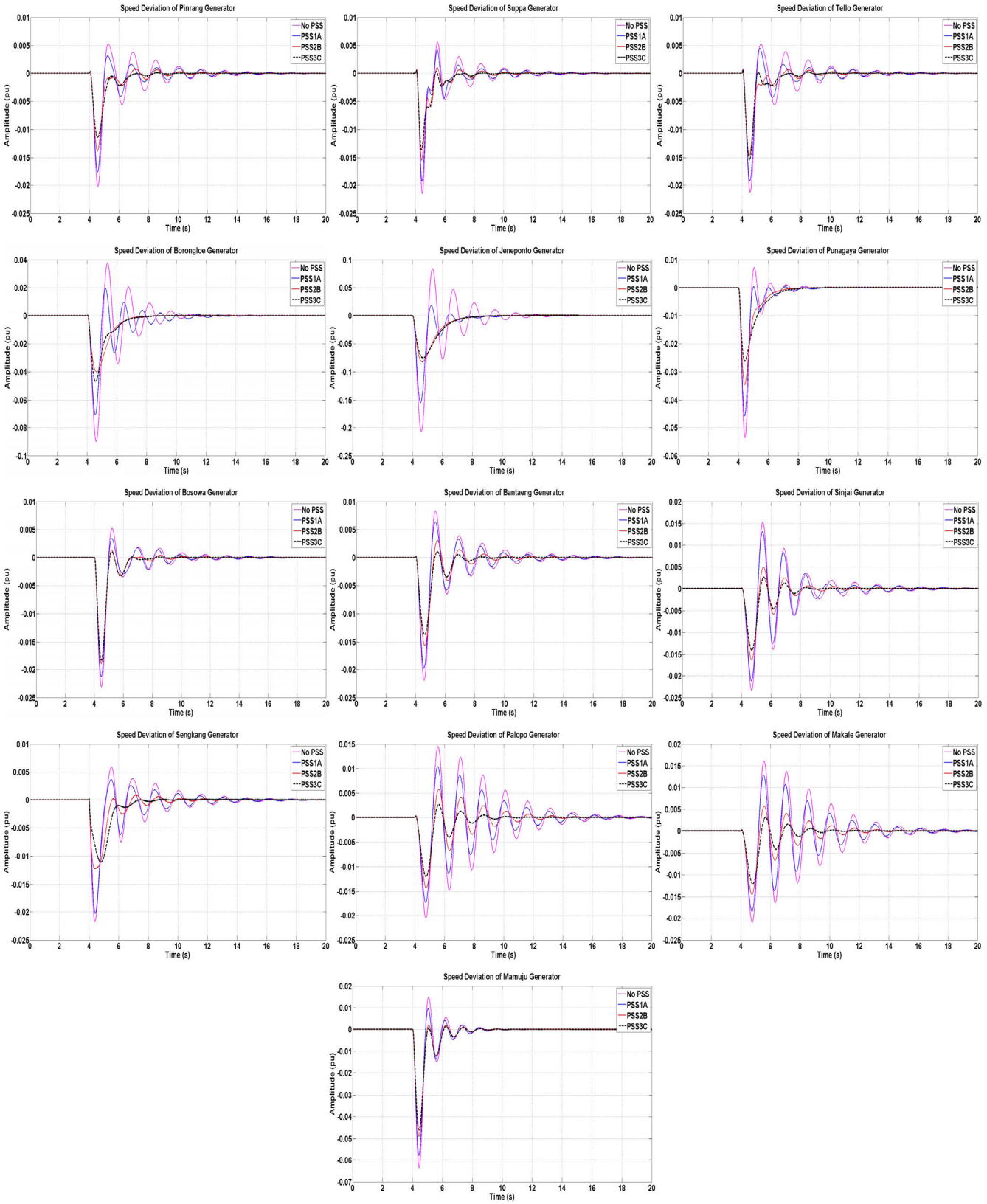

FIGURE 14. Comparison of $\Delta\omega$ response in various generators.

TABLE 10. Speed overshoot response.

G	No PSS(pu)	PSS1A(pu)	PSS2B(pu)	PSS3C(pu)
Bakaru	-0.01953 & 0.004698	-0.01629 & 0.002019	-0.01183 & 0.0009272	-0.009859 & 0.0002462
Pinrang	-0.02022 & 0.005278	-0.01755 & 0.003143	-0.01381 & 0.0008197	-0.0114 & 0.0003213
Suppa	-0.02143 & 0.005582	-0.0193 & 0.004174	-0.01547 & 0.001028	-0.0136 & 0.000521
Tello	-0.0212 & 0.005225	-0.01921 & 0.004456	-0.0147 & 0.0006909	-0.01545 & 0.000577
Borongloe	-0.08983 & 0.03765	-0.07048 & 0.01961	-0.04002 & 0.0003252	-0.04707 & 0.0003086
PLTU Jeneponto	-0.2069 & 0.08389	-0.1548 & 0.01798	-0.08251 & 0.0005185	-0.0755 & 0.0004634
PLTU Punagaya	-0.0535 & 0.007202	-0.04564 & 0.0004313	-0.03449 & 6.871e-05	-0.02629 & 0.0001035
PLTU Bosowa	-0.02308 & 0.005201	-0.0213 & 0.00339	-0.01885 & 0.001363	-0.01823 & 0.001056
Bantaeng	-0.02192 & 0.008359	-0.01977 & 0.006408	-0.01566 & 0.003088	-0.01375 & 0.00107
Sinjai	-0.02327 & 0.01531	-0.02118 & 0.01313	-0.01627 & 0.004956	-0.01403 & 0.002599
WPP Sidrap	-0.02209 & 0.009257	-0.01652 & 0.003408	-0.01459 & 0.001624	-0.01354 & 0.001937
Sengkang	-0.02173 & 0.005916	-0.0203 & 0.003665	-0.01222 & 0.0009451	-0.01112 & 0.0002353
Palopo	-0.02055 & 0.01451	-0.01728 & 0.01041	-0.01434 & 0.005751	-0.01207 & 0.00265
Makale	-0.02093 & 0.01612	-0.01845 & 0.01285	-0.01445 & 0.005723	-0.01208 & 0.003148
Mamuju	-0.06349 & 0.01479	-0.05793 & 0.009475	-0.04893 & 0.002038	-0.0461 & 0.001313

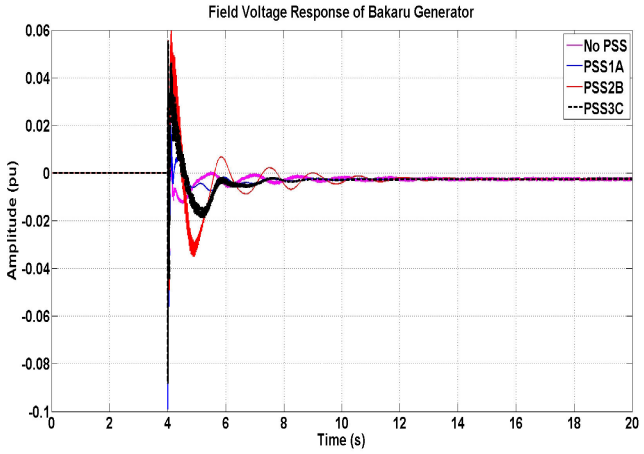

FIGURE 15. Comparison of E_{fd} response in bakaru generator.

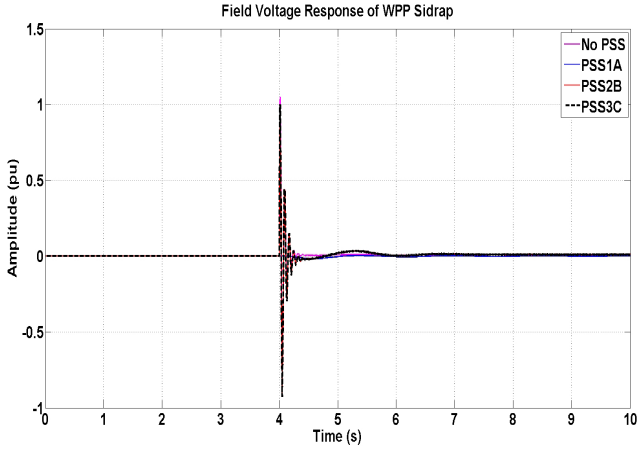

FIGURE 16. Comparison of E_{fd} response in WPP generator.

was 16.23 seconds without additional control. The application of PSS1A reduced the settling time to 14.42 seconds. With PSS2B, the settling time further improves to 10.96 seconds, whereas with PSS3C, it decreased to 9.347 seconds. These findings demonstrate the effectiveness of PSS3C in significantly accelerating the settling time of a WPP SIDRAP

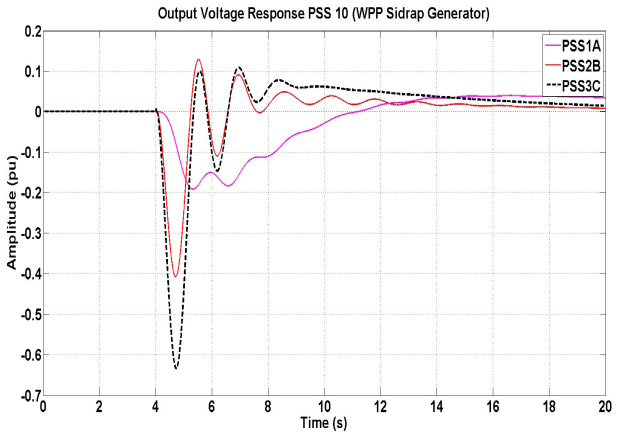

FIGURE 17. Comparison of V_{PSS} response in WPP generator.

generator. Table 11 provides a comprehensive evaluation of the settling times across different control techniques and compare the performance of the generators under various strategies.

2) EIGENVALUE ANALYSIS

This section examine the eigenvalue systems of power systems under different control schemes, encompassing scenarios without PSS, with PSS1A, PSS2B, and PSS3C. The analysis included critical eigenvalues (Table 12), inter-area system eigenvalues (Table 13), and local system eigenvalues (Table 14). These tables provide insightful information regarding the impact of different control strategies on eigenvalue system behavior. The analysis demonstrated how different control techniques can enhance the eigenvalue system. This improvement is discernible in the leftward shift of the eigenvalues, indicating a more negative real part (σ), thereby enhancing system stability. Notably, the efficacy of MB-PSS3C in improving the eigenvalue and damping system is highlighted, as evidenced by the more negative eigenvalues presented in the table. These enhanced eigenvalues play a crucial role in improving the overall stability and performance of the system.

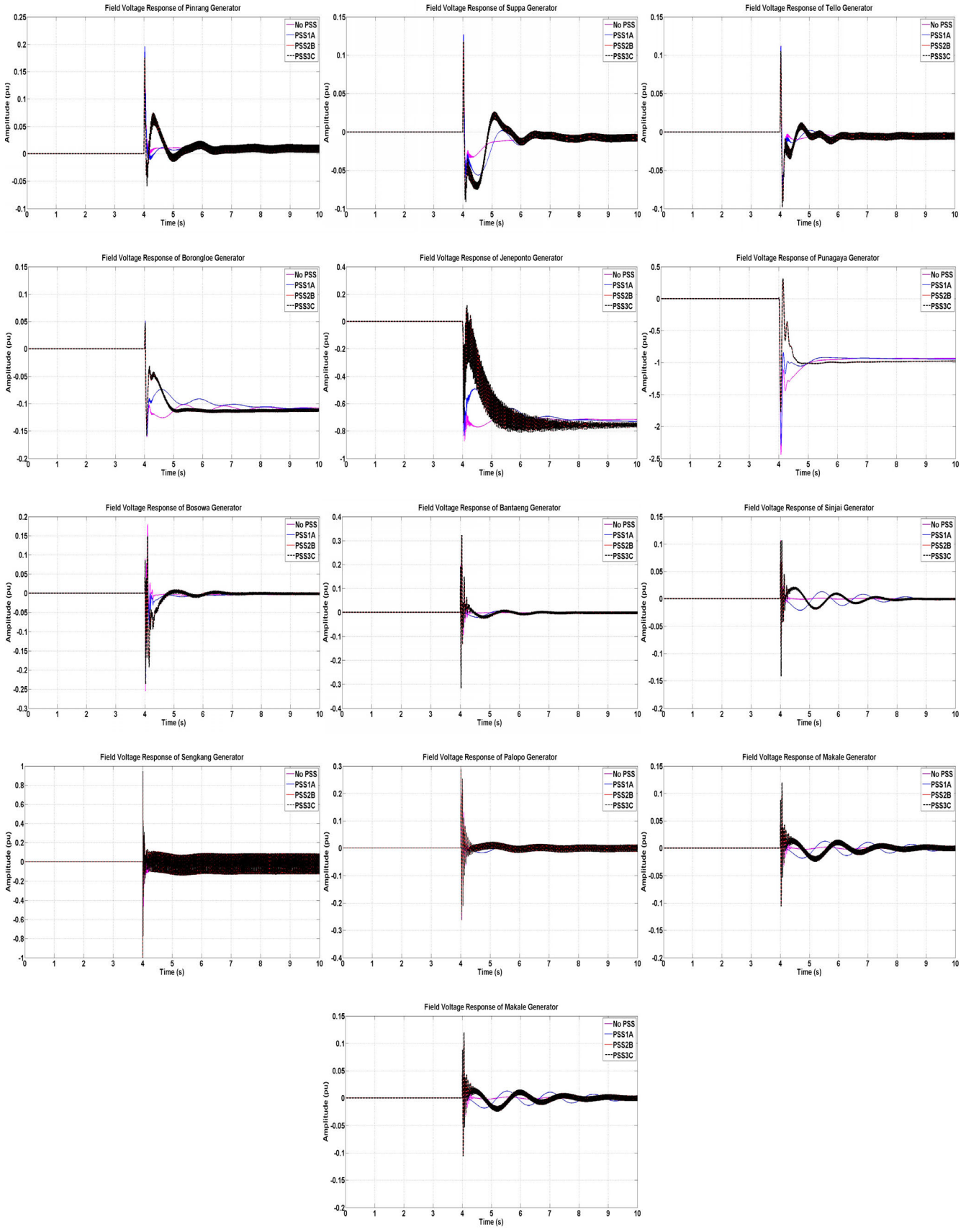

FIGURE 18. Comparison of E_{fd} response in various generators.

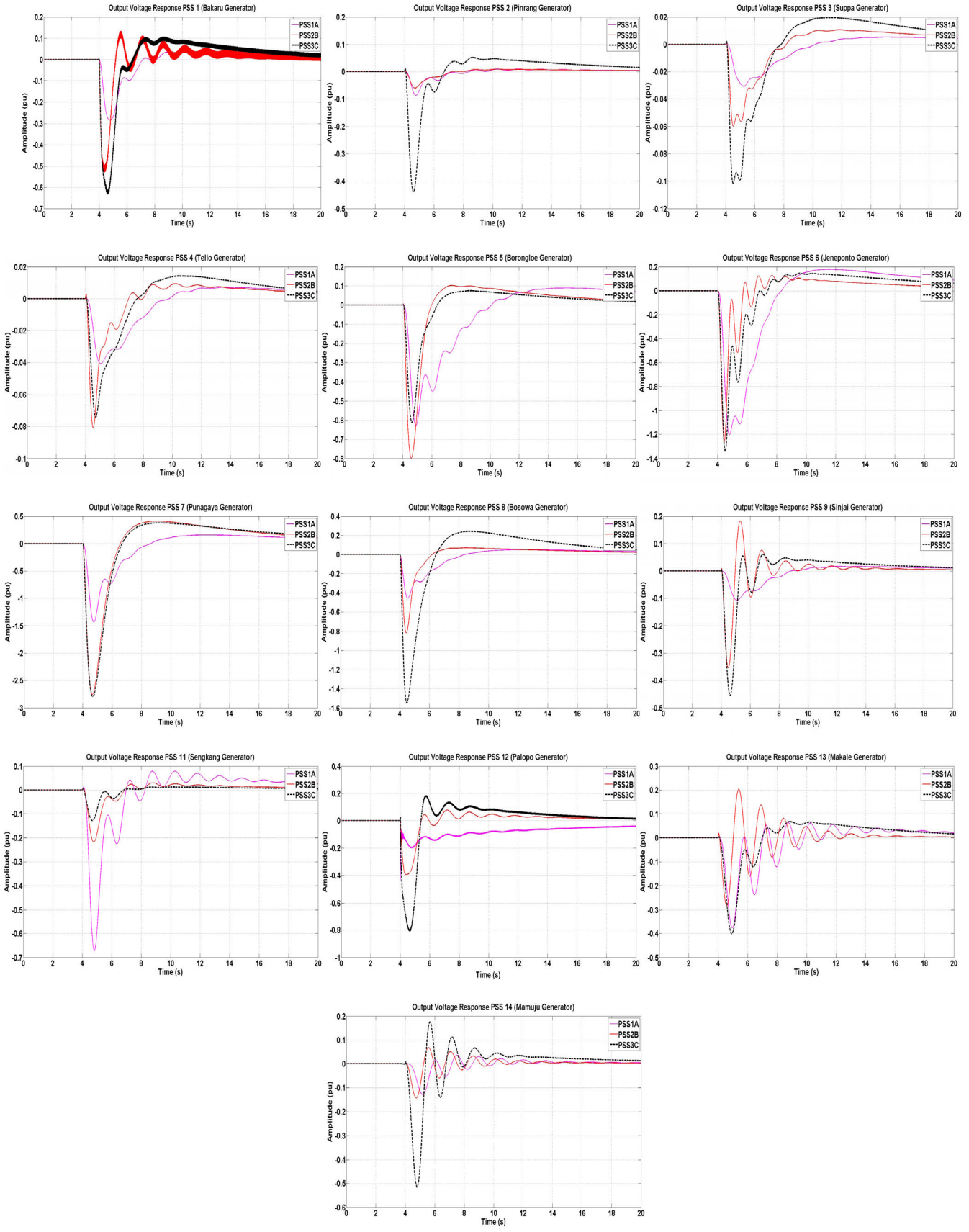

FIGURE 19. Comparison of V_{pss} response in various generators.

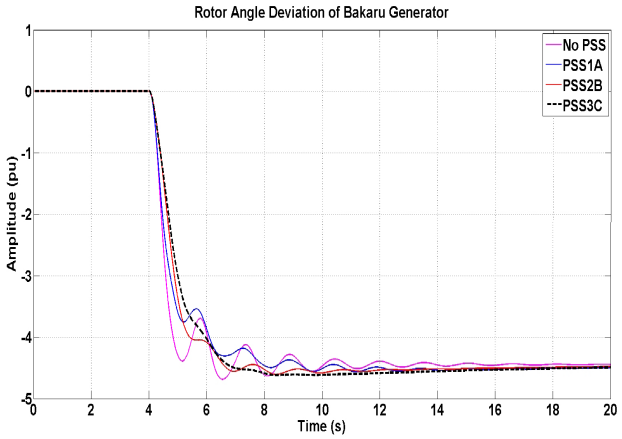

FIGURE 20. Comparison of $\Delta\delta$ response in bakaru generator.

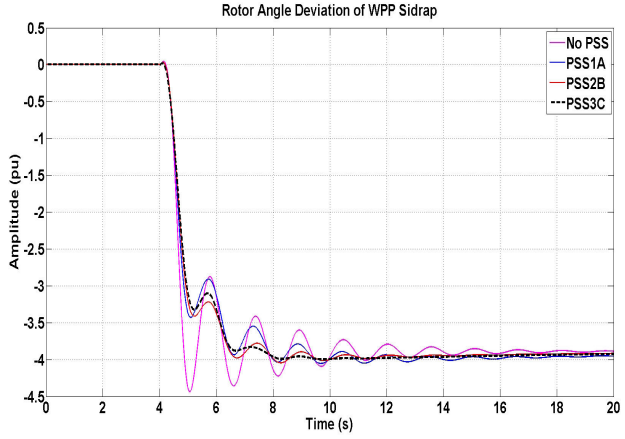

FIGURE 21. Comparison of $\Delta\delta$ response in WPP generator.

C. DISCUSSION

This research analyzes the increase in the stability of the Sulselrabar system resulting from WPP penetration. It proposes the application of MB-PSS3C based on MOA artificial intelligence, utilizing the latest system data. In general, the analysis is carried out using several system operating schemes and Swarm Intelligence-based optimization methods, including

- SB-PSS1A based on PSO, FA, and MOA.
- MB-PSS2B based on PSO, FA, and MOA.
- MB-PSS3C based on PSO, FA, and MOA.

1) MOA PERFORMANCE

The performance was evaluated using a convergence performance analysis and benchmarking. The population-based MOA approach offers significant advantages, drawing inspiration from the behavior of adult mayflies. It incorporates processes such as crossing, mutation, swarm gathering, mating dances, and random walking, which contribute to its exploration capability. This method enhances exploration by employing two distinct equations for each population (male and female mayflies). When compared with similar swarm intelligence algorithms, such as PSO and FA, both of which are considered high-quality metaheuristic optimization algorithms, MOA demonstrates superior performance, particularly in terms of local and global search capabilities. This method exhibited a higher probability of finding the global optimum point. In additionally, the remarkable convergence behavior of the proposed MOA method often yields the best overall solution in the initial iterations.

TABLE 11. $\Delta\delta$ settling time response.

G	No PSS(s)	PSS1A(s)	PSS2B(s)	PSS3C(s)
Bakaru	17.74	13.6	10.75	8.454
Pinrang	17.37	14.17	12.05	9.73
Suppa	15.4	13.59	10.81	9.209
Tello	16.31	14.36	10.43	9.253
Borongloe	15.71	12.29	7.94	7.665
PLTUjnpto	13.34	10.19	7.918	7.612
PLTUpngya	13.63	9.73	7.692	7.509
PLTUbsw	16.18	14.07	9.075	8.047
Bantaeng	17.52	15.07	11.93	8.669
Sinjai	17.62	15.48	12.78	9.114
WPPSidrap	16.23	14.42	10.96	9.347
Sengkang	17.81	15.81	10.64	8.242
Palopo	18.89	15.59	13.39	9.57
Makale	19.47	16.87	13.16	9.728
Mamuju	12.06	10.39	8.481	8.247

2) MB-PSS3C PERFORMANCE

MB-PSS is primarily designed to absorb disturbances within the electrical network, which can induce electromechanical oscillations in the power system. MB-PSS offers support across three distinct frequency bands: high-frequency, medium-frequency, and low-frequency band modes. The low-band mode specifically addresses slow oscillations within an isolated system. The intermediate band addresses oscillations occurring between regional network frequencies, typically ranging from 0.2 Hz to 1.0 Hz, which refers to fluctuations within a specific geographic area. Meanwhile, the high band targets local or inter-machine oscillations, such as those between the alternator and other machines within the same generator, within the frequency range of 0.8 Hz to 4.0 Hz.

Disturbances within the power system induce various electromechanical oscillation modes in generators, subsequently influencing the stability of the power system and transmission limits. Electromechanical oscillations typically occur within the frequency range of 0.04 to 4.0 Hz and manifest in three main types: local (interunit and interstation), inter-area, and system-wide oscillations. The MB-PSS is equipped with settings for three distinct frequency bands, enabling flexible adjustment of its response to accommodate various electromechanical oscillation modes present in the main power system. This flexibility enhances the dynamic and transient stability of the electric power system, thereby making it more robust. The MB-PSS3C designed in this study, effectively dampened all oscillation modes, contributing to improved stability.

3) OPTIMIZATION PERFORMANCE

Analysis of the increase in stability of the Sulselrabar system due to WPP penetration was carried out using several analytical methods, including

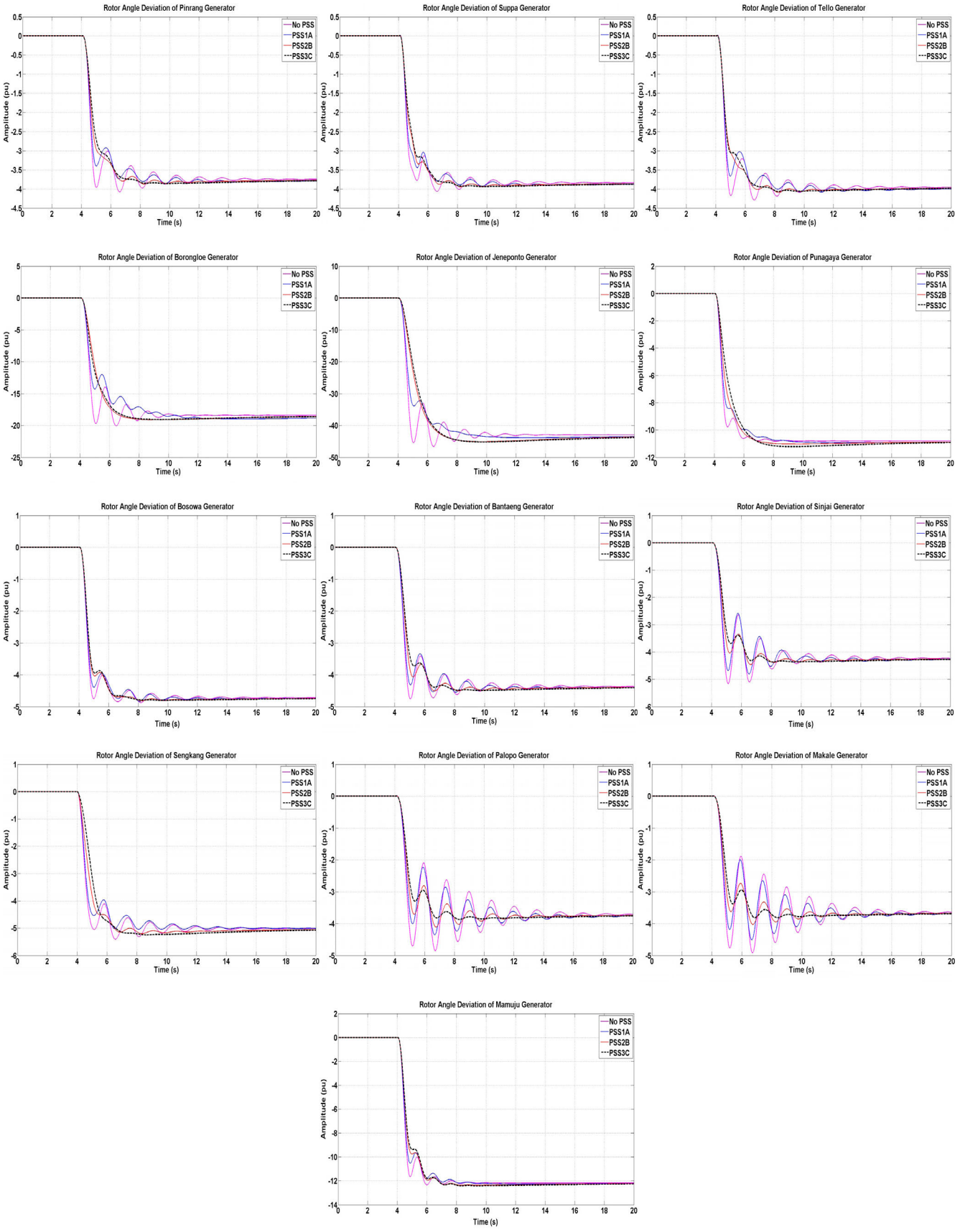

FIGURE 22. Comparison of $\Delta\delta$ response in various generators.

TABLE 12. Critical eigenvalue system.

No PSS(pu) 1.0 e+02	PSS1A(pu) 1.0 e+02	PSS2B(pu) 1.0 e+02	PSS3C(pu) 1.0 e+02
-0.5215+6.5549i	-0.4518+5.1220i	-0.5168+6.5596i	-0.5103+6.5295i
-0.5215-6.5549i	-0.4518-5.1220i	-0.5168-6.5596i	-0.5103-6.5295i
-0.4436+5.3198i	-0.3062+4.6949i	-0.4414+5.3010i	-0.4385+5.2480i
-0.4436-5.3198i	-0.3062-4.6949i	-0.4414-5.3010i	-0.4385-5.2480i
-0.4142+5.0621i	-0.3192+4.5401i	-0.4064+5.0502i	-0.3732+4.9996i
-0.4142-5.0621i	-0.3192-4.5401i	-0.4064-5.0502i	-0.3732-4.9996i
-0.3056+4.6945i	-0.2132+4.5199i	-0.3062+4.6970i	-0.3053+4.6949i
-0.3056-4.6945i	-0.2132-4.5199i	-0.3062-4.6970i	-0.3053-4.6949i
-0.3139+4.5323i	-0.1366+4.3431i	-0.3241+4.5266i	-0.3193+4.5303i
-0.3139-4.5323i	-0.1366-4.3431i	-0.3241-4.5266i	-0.3193-4.5303i
-0.1973+4.4653i	-0.1965+4.3137i	-0.1907+4.4437i	-0.1691+4.3794i
-0.1973-4.4653i	-0.1965-4.3137i	-0.1907-4.4437i	-0.1691-4.3794i
-0.1280+4.3272i	-0.0925+4.1576i	-0.1371+4.2800i	-0.1959+4.3151i
-0.1280-4.3272i	-0.0925-4.1576i	-0.1371-4.2800i	-0.1959-4.3151i
-0.0857+4.1565i	-0.2612+4.1960i	-0.1970+4.3149i	-0.1331+4.2704i
-0.0857-4.1565i	-0.2612-4.1960i	-0.1970-4.3149i	-0.1331-4.2704i
-0.1965+4.3135i	-0.0412+3.9001i	-0.2794+4.2210i	-0.2824+4.2253i
-0.1965-4.3135i	-0.0412-3.9001i	-0.2794-4.2210i	-0.2824-4.2253i
-0.0413+3.9001i	-0.0811+4.0459i	-0.0412+3.9001i	-0.0413+3.9001i
-0.0413-3.9001i	-0.0811-4.0459i	-0.0412-3.9001i	-0.0413-3.9001i
-0.2596+4.1937i	-0.0303+3.5666i	-0.0172+4.0844i	-0.0287+4.1012i
-0.2596-4.1937i	-0.0303-3.5666i	-0.0172-4.0844i	-0.0287-4.1012i
-0.0808+4.0453i	-0.0921+2.3021i	-0.0801+4.0465i	-0.0803+4.0472i
-0.0808-4.0453i	-0.0921-2.3021i	-0.0801-4.0465i	-0.0803-4.0472i
-0.0303+3.5670i	1.6885+0.0000i	-0.0305+3.5614i	-0.0310+3.5626i
-0.0303-3.5670i	-0.1188+1.3768i	-0.0305-3.5614i	-0.0310-3.5626i
-0.0988+2.3043i	-0.1188-1.3768i	-0.0167+2.2826i	-0.0035+2.2798i
-0.0988-2.3043i	-0.0032+0.0414i	-0.0167-2.2826i	-0.0035-2.2798i
1.6912+0.0000i	-0.0032-0.0414i	1.6621+0.0000i	1.6667+0.0000i
-0.1488+1.5168i	-0.0043+0.0463i	-0.1418+1.5091i	-0.1390+1.5068i
-0.1488-1.5168i	-0.0043-0.0463i	-0.1418-1.5091i	-0.1390-1.5068i
-0.1171+1.3752i		-0.1044+1.3640i	-0.1137+1.3705i
-0.1171-1.3752i		-0.1044-1.3640i	-0.1137-1.3705i
-0.0033+0.0409i		0.0062+0.0651i	0.0034+0.0619i
-0.0033-0.0409i		0.0062-0.0651i	0.0034-0.0619i
-0.0044+0.0462i			
-0.0044-0.0462i			

TABLE 13. Inter-area eigenvalue system.

No PSS(pu) 1.0 e+02	PSS1A(pu) 1.0 e+02	PSS2B(pu) 1.0 e+02	PSS3C(pu) 1.0 e+02
-0.3305+4.0947i	-0.5205+5.0016i	-4.1029+2.7371i	-4.3285+2.3423i
-0.4444+4.6227i	-0.3164+4.1394i	-3.0040+4.3719i	-0.8257+4.5882i
-0.5102+4.5222i	-0.4257+4.6305i	-3.8630+3.1082i	-0.7492+4.0388i
-0.5138+4.5350i	-0.8758+4.8344i	-0.6334+4.5714i	-2.1300+2.3451i
		-0.4361+4.0779i	

- Damping Analysis
- Time-domain simulation: speed deviation, field voltage, PSS output voltage, and rotor angle response for each generator
- Eigenvalue Analysis

Based on the damping analysis results, the maximum damping was obtained with the implementation of MOA-based MB-PSS3C. MB-PSS3C provides maximum damping, which is important for improving the oscillation stability performance of the power system, especially during WPP penetration. The time-domain simulation analysis included observations of the speed response, field voltage response, PSS output voltage response, and rotor angle response for each generator. This analysis assesses parameters such as overshoot response and settling time.

Based on the speed response, field voltage response, PSS output voltage response, and rotor angle response of the generators, it is observed that an additional load results in electrical power (P_e) exceeding the mechanical power (P_m), as indicated by $P_e > P_m$. The responses obtained from the generators during the load change disturbances were downward or negative, indicating a decrease in certain parameters. Load change disturbances were applied to the WPP SIDRAP and BAKARU generators. In this scenario, the primary role of the PSS is to mitigate the oscillations that occur, ensuring that the stability of the Sulselrabar system is maintained. The adoption of the MOA-based

TABLE 14. Local eigenvalue system.

No PSS(pu) 1.0 e+02	PSS1A(pu) 1.0 e+02	PSS2B(pu) 1.0 e+02	PSS3C(pu) 1.0 e+02
-1.0213+9.0136i	-1.0308+9.1684i	-1.2092+8.9756i	-1.2043+9.1708i
-0.9048+7.9629i	-1.0211+8.2608i	0.6189+6.5081i	-5.4460+6.8174i
-1.0650+7.0789i	-1.1922+7.1392i	-3.4840+6.4997i	0.3432+6.1905i
-0.8519+6.8855i	-0.9873+6.5415i	-1.8208+6.4342i	-2.0938+6.1358i
-1.4630+6.2015i	-1.4845+6.2640i	-1.2536+5.8688i	-3.3978+5.3573i
-0.7857+5.3370i	-1.3885+6.0100i	-2.2254+5.6222i	-1.1956+5.7865i
-0.9336+5.5104i	-0.9234+5.6633i	-1.0082+5.5213i	-2.1460+5.2102i
-1.0967+5.8258i	-1.2344+5.7325i	-0.9859+5.3987i	-1.0438+5.4854i
-1.2476+5.8275i	-1.4196+5.8714i	-1.3045+5.3270i	-1.0304+5.3554i
-1.1490+5.6579i	-1.1397+5.6802i	-1.4311+5.0708i	-1.5626+5.4704i
-1.1518+5.6619i	-0.8146+5.3741i		-1.7359+5.3721i

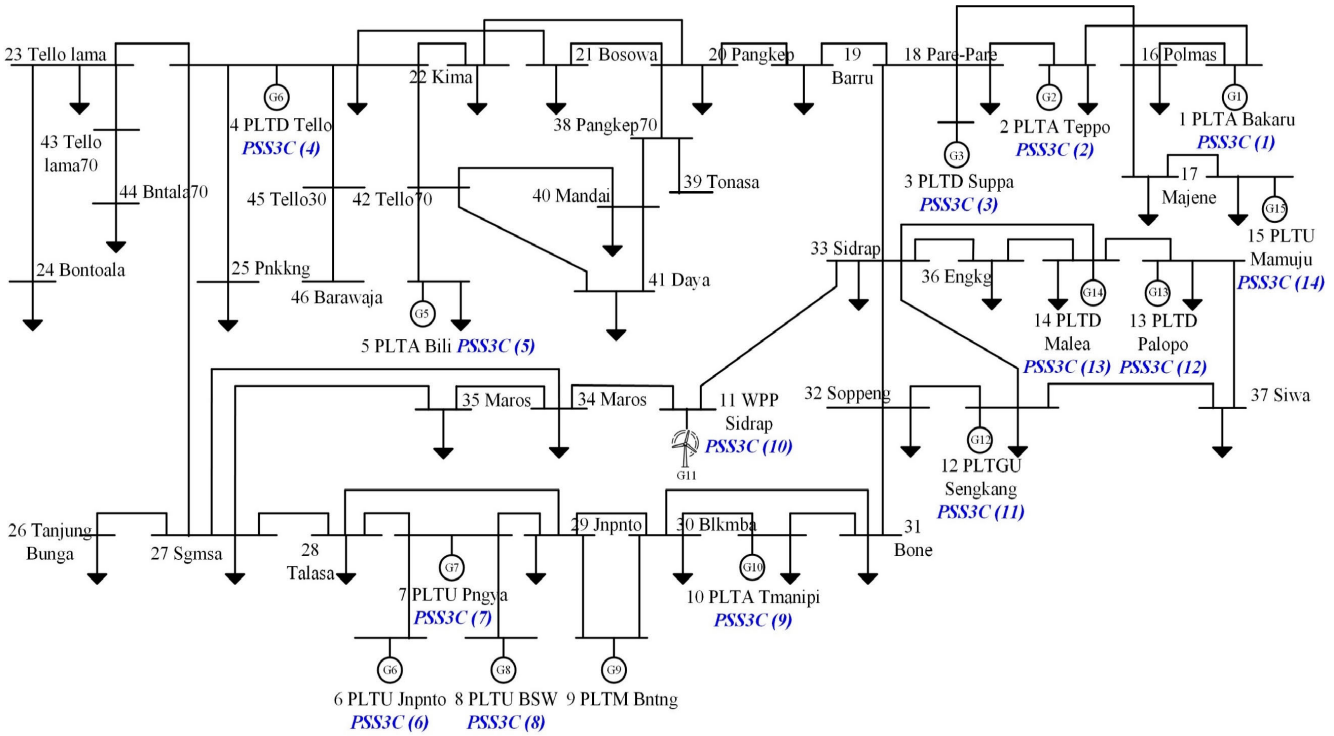

FIGURE 23. Single-line diagram of the sulselrabar system post-optimization.

MB-PSS3C control strategy resulted in several improvements in the system stability, including a decrease in the minimum overshoot response, quicker settling time response, and a shift towards more negative eigenvalues. Settling time refers to the time required for a system to return to a steady state after experiencing a disturbance. A faster settling time indicates a more rapid response, which indicates improved stability.

The Sulselrabar single-line diagram system, as depicted in Fig. 23, illustrates the utilization of the MOA approach for optimizing the placement of MB-PSS3C. The optimized placement ensures effective integration of MB-PSS3C within the Sulselrabar electric power system. Additionally, the integration of WPP SIDRAP renewable generators into the system enhances the line flow and reduces system losses by leveraging renewable energy sources.

4) CHALLENGES AND STRATEGY

Currently, the Sulselrabar system comprises a mix of thermal generators and generators from renewable energy sources such as hydro power and wind power. Looking ahead, there is a growing emphasis on prioritizing renewable energy generation, especially from WPP. This shift was supported by government initiatives aimed at increasing electricity generation from renewable sources. Hence, there is a need for control device technology that enhances the system performance, particularly in light of WPP penetration. In addition, it is crucial to anticipate the dynamics of consumer load development. The Sulselrabar system is among the largest in Indonesia, linking major load centers across four provinces: South, Southeast, and West Sulawesi. In the future, the Sulselrabar system is expected to become more extensive and complex with the expansion of its coverage area to include

Central and North Sulawesi. Sulawesi Island has the highest wind energy potential in Indonesia, making the development of WPP in this area strategically important.

The preliminary results of this study indicate that the penetration of renewable energy generation affects the stability of the system. Additionally, variations in the system load also significantly influence the stability of the Sulselrabar system by altering the power flow. Current control systems in generators, such as AVR and excitation systems, are unable to effectively overcome instability owing to their limited functionalitys. Hence, it is necessary to equip the Sulselrabar system with additional PSS controls to mitigate instability. This research suggests implementing MB-PSS3C based on MOA artificial intelligence, which offers maximum influence to the generators in the Sulselrabar system by optimizing their responses to disturbances. For future research on the Sulselrabar system, integrating MOA-based MB-PSS3C with other control equipment, such as FACTS devices, could be explored to further enhance the system stability.

V. CONCLUSION

This study recommends the use of the Mayfly Optimization Algorithm (MOA) for optimizing both the location and parameters of the Multi-Band Power System Stabilizer type MB-PSS3C in the Sulselrabar system integrated with the Wind Power Plant (WPP) SIDRAP. The optimal installation location for the MB-PSS3C among the 14 generators was identified, and the MOA approach was employed to optimize its parameters. The application of MB-PSS3C, based on MOA, demonstrated superior outcomes compared to alternative control techniques. These outcomes include improved system eigenvalues, reduced overshoot oscillation, quick settling time, and ideal generator field voltage response. The increase in the damping system is associated with an enhancement in the system stability. The incorporation of 14 MOA-based Multi-Band Power System Stabilizer type MB-PSS3C units resulted in the highest damping ratio, reaching 0.7498925. The MOA technique exhibited efficiency by achieving a minimum fitness function value of 80.4372791 at the thirteenth iteration. These findings suggest that, in comparison to Particle Swarm Optimization (PSO) approaches, the MOA method computes a minimal fitness function value more swiftly.

In future work, there are several topics that can be researched both related to the Sulselrabar system and other systems, namely,

1) Integration of MOA-based MB-PSS3C with other control equipment: This study explores the potential benefits of integrating MOA-based MB-PSS3C controllers with FACTS devices to enhance the stability of the Sulselrabar power system and other large-scale multi-machine systems.
2) Further investigation into MOA implementation: This topic focuses on evaluating the efficiency and effectiveness of MOA in addressing various engineering optimization problems beyond power systems. It also suggests comparing the MOA with other optimization algorithms to assess its performance and versatility.
3) Implementation of MOA-based MB-PSS3C in other electric power systems: This study suggests extending the application of MOA-based MB-PSS3C to other electric power systems, particularly those with renewable energy integration, such as solar and wind power plants.

REFERENCES

[1] D. Zhou, F. Hu, S. Wang, and J. Chen, "Power network robustness analysis based on electrical engineering and complex network theory," *Phys. A, Stat. Mech. Appl.*, vol. 564, Feb. 2021, Art. no. 125540, doi: 10.1016/j.physa.2020.125540.

[2] N. Mlilo, J. Brown, and T. Ahfock, "Impact of intermittent renewable energy generation penetration on the power system networks—A review," *Technol. Econ. Smart Grids Sustain. Energy*, vol. 6, no. 1, p. 25, Dec. 2021, doi: 10.1007/s40866-021-00123-w.

[3] N. Hatziargyriou, J. Milanovic, C. Rahmann, V. Ajjarapu, C. Canizares, I. Erlich, D. Hill, I. Hiskens, I. Kamwa, B. Pal, P. Pourbeik, J. Sanchez-Gasca, A. Stankovic, T. Van Cutsem, V. Vittal, and C. Vournas, "Definition and classification of power system stability—Revisited & extended," *IEEE Trans. Power Syst.*, vol. 36, no. 4, pp. 3271–3281, Jul. 2021, doi: 10.1109/TPWRS.2020.3041774.

[4] J. Luo, F. Teng, and S. Bu, "Stability-constrained power system scheduling: A review," *IEEE Access*, vol. 8, pp. 219331–219343, 2020, doi: 10.1109/ACCESS.2020.3042658.

[5] M. A. Prakasa, I. Robandi, R. Nishimura, and M. R. Djalal, "A new scheme of Harris hawk optimizer with memory saving strategy (HHO-MSS) for controlling parameters of power system stabilizer and virtual inertia in renewable microgrid power system," *IEEE Access*, early access, Apr. 4, 2024, doi: 10.1109/ACCESS.2024.3385089.

[6] D. Y. Yang, L. Wang, G. Cai, Z. Chen, J. Ma, B. Wang, and Z. Sun, "Synchronized ambient output-only based online inter-area transfer capability assessment considering small signal stability," *IEEE Trans. Power Syst.*, vol. 36, no. 1, pp. 261–270, Jan. 2021, doi: 10.1109/TPWRS.2020.3004838.

[7] A. A. Alsakati, C. A. Vaithilingam, J. Alnasseir, and A. Jagadeeshwaran, "Investigation of single-band and multi-band power system stabilizers towards transient stability improvement in electrical networks," in *Proc. IEEE Conf. Energy Convers. (CENCON)*, Oct. 2021, pp. 196–201, doi: 10.1109/CENCON51869.2021.9627246.

[8] M. M. Eladany, A. A. Eldesouky, and A. A. Sallam, "Power system transient stability: An algorithm for assessment and enhancement based on catastrophe theory and FACTS devices," *IEEE Access*, vol. 6, pp. 26424–26437, 2018, doi: 10.1109/ACCESS.2018.2834906.

[9] S. U. Kakaiya, O. Cephas, G. N. Paichaure, and B. R. Parekh, "Enhancement of power system stability using FACTS devices," *Int. J. Comput. Sci. Eng.*, vol. 6, no. 12, pp. 542–546, Dec. 2018, doi: 10.26438/ijcse/v6i12.542546.

[10] J. Bhukya and V. Mahajan, "Optimization of controllers parameters for damping local area oscillation to enhance the stability of an interconnected system with wind farm," *Int. J. Electr. Power Energy Syst.*, vol. 119, Jul. 2020, Art. no. 105877, doi: 10.1016/j.ijepes.2020.105877.

[11] W. Peres and N. N. da Costa, "Comparing strategies to damp electromechanical oscillations through STATCOM with multi-band controller," *ISA Trans.*, vol. 107, pp. 256–269, Dec. 2020, doi: 10.1016/j.isatra.2020.08.005.

[12] O. M. Benaissa, S. Hadjeri, and S. A. Zidi, "Impact of PSS and SVC on the power system transient stability," in *Proc. 8th Int. Conf. Model., Identificat. Control (ICMIC)*, Nov. 2016, pp. 303–307, doi: 10.1109/ICMIC.2016.7804127.

[13] S. S. Bhole and P. Nigam, "Improvement of voltage stability in power system by using SVC and STATCOM," *Int. J. Adv. Res. Electr., Electron. Instrum. Eng.*, vol. 4, no. 2, pp. 749–755, Feb. 2015, doi: 10.15662/ijareeie.2015.0402035.

[14] P. Dey, S. Mitra, A. Bhattacharya, and P. Das, "Comparative study of the effects of SVC and TCSC on the small signal stability of a power system with renewables," *J. Renew. Sustain. Energy*, vol. 11, no. 3, May 2019, Art. no. 033305, doi: 10.1063/1.5085066.

[15] M. R. Shakarami and I. Faraji Davoudkhani, "Wide-area power system stabilizer design based on grey wolf optimization algorithm considering the time delay," *Electric Power Syst. Res.*, vol. 133, pp. 149–159, Apr. 2016, doi: 10.1016/j.epsr.2015.12.019.

[16] Y. Welhazi, T. Guesmi, B. M. Alshammari, K. Alqunun, A. Alateeq, Y. Almalaq, R. Alsabhan, and H. H. Abdallah, "A novel hybrid chaotic Jaya and sequential quadratic programming method for robust design of power system stabilizers and static VAR compensator," *Energies*, vol. 15, no. 3, p. 860, Jan. 2022, doi: 10.3390/en15030860.

[17] G. Yu, T. Lin, J. Zhang, Y. Tian, and X. Yang, "Coordination of PSS and FACTS damping controllers to improve small signal stability of large-scale power systems," *CSEE J. Power Energy Syst.*, vol. 5, no. 4, pp. 507–514, Dec. 2019, doi: 10.17775/CSEEJPES.2018.00530.

[18] N. Nikolaev, "Tuning of power system stabilizer PSS3B and analysis of its properties," in *Proc. 20th Int. Symp. Electr. App. Technol. (SIELA)*, Jun. 2018, pp. 1–5, doi: 10.1109/SIELA.2018.8447166.

[19] L. Hajagos and M. Basler, "Changes to IEEE 421.5 recommended practice for excitation system models for power system stability studies," in *Proc. IEEE Power Eng. Soc. General Meeting*, Jun. 2005, pp. 334–336, doi: 10.1109/IEEESTD.1992.106975.

[20] *IEEE Recommended Practice for Excitation System Models for Power System Stability Studies*, IEEE Standard 421.5-2016 (Revision of IEEE Std 421.5-2005), 2016, pp. 1–207, doi: 10.1109/IEEESTD.2016.7553421.

[21] R. Khezri, A. Oshnoei, A. Yazdani, and A. Mahmoudi, "Intelligent coordinators for automatic voltage regulator and power system stabiliser in a multi-machine power system," *IET Gener., Transmiss. Distribution*, vol. 14, no. 23, pp. 5480–5490, Dec. 2020, doi: 10.1049/iet-gtd.2020.0504.

[22] S. K. Mohapatra, M. K. Senapati, and S. K. Dash, "Coordinated design of PSS and AVR for stability enhancement using differential evolution algorithm," in *Proc. Sixth Int. Conf. Intell. Comput. Appl. ICICA*. Singapore: Springer, 2021, pp. 387–396, doi: 10.1007/978-981-16-1335-7_35.

[23] R. Wang, X. Liu, and Y. Huang, "Synchronous generator excitation system for a ship based on active disturbance rejection control," *Math. Problems Eng.*, vol. 2021, pp. 1–17, Apr. 2021, doi: 10.1155/2021/6638370.

[24] J. J. Kim and J. H. Park, "A novel structure of a power system stabilizer for microgrids," *Energies*, vol. 14, no. 4, p. 905, Feb. 2021, doi: 10.3390/en14040905.

[25] A. Khodabakhshian and R. Hemmati, "Multi-machine power system stabilizer design by using cultural algorithms," *Int. J. Electr. Power Energy Syst.*, vol. 44, no. 1, pp. 571–580, Jan. 2013, doi: 10.1016/j.ijepes.2012.07.049.

[26] Z. Seddiki, T. Allaoui, M. Bey, and M. Denai, "Combining multi-band power system stabilizers and hybrid power flow controllers to support electricity grids with high penetration of distributed renewable generation," *Indonesian J. Electr. Eng. Informat. (IJEEI)*, vol. 10, no. 2, pp. 441–451, May 2022, doi: 10.52549/ijeei.v10i2.3666.

[27] M. Fan, K. Wang, and J. Zhang, "Parameters setting of power system stabilizer PSS2B," in *Proc. 4th Int. Conf. Renewable Energy Environ. Technol.*, 2017, pp. 63–70, doi: 10.2991/icreet-16.2017.12.

[28] A. Khujaev, C. A. Vaithilingam, A. A. Alsakati, and J. Alnasseir, "Stability enhancement of power system with the implementation of power system stabilizer PSS and excitation system IEEE type-1," *J. Phys., Conf.*, vol. 2120, no. 1, Dec. 2021, Art. no. 012022, doi: 10.1088/1742-6596/2120/1/012022.

[29] A. A. Alsakati, C. A. Vaithilingam, K. Naidu, G. Rajendran, J. Alnasseir, and A. Jagadeeshwaran, "Particle swarm optimization for tuning power system stabilizer towards transient stability improvement in power system network," in *Proc. IEEE Int. Conf. Artif. Intell. Eng. Technol. (IICAIET)*, Sep. 2021, pp. 1–6, doi: 10.1109/IICAIET51634.2021.9573534.

[30] P. Maric, R. Kljajic, H. R. Chamorro, and H. Glavas, "Power system stabilizer tuning algorithm in a multimachine system based on S-domain and time domain system performance measures," *Energies*, vol. 14, no. 18, p. 5644, Sep. 2021, doi: 10.3390/en14185644.

[31] M. Y. Yunus, M. R. Djalal, and M. Marhatang, "Optimal design power system stabilizer using firefly algorithm in interconnected 150 kV sulselrabar system, Indonesia," *Int. Rev. Electr. Eng. (IREE)*, vol. 12, no. 3, p. 250, Jun. 2017, doi: 10.15866/iree.v12i3.11136.

[32] J. Morsali, "TID-based PSS2B to overcome LFO issue in multi-machine power systems," in *Proc. 30th Int. Conf. Electr. Eng. (ICEE)*, May 2022, pp. 968–973, doi: 10.1109/ICEE55646.2022.9827003.

[33] M. R. Djalal, I. Robandi, and M. A. Prakasa, "Stability enhancement of sulselrabar electricity system using mayfly algorithm based on static var compensator and multi-band power system stabilizer PSS2B," *IEEE Access*, vol. 11, pp. 57319–57340, 2023, doi: 10.1109/ACCESS.2023.3283598.

[34] M. Ahmadi Kamarposhti, H. Shokouhandeh, Y. Gholami Omali, I. Colak, P. Thounthong, and W. Holderbaum, "Optimal coordination of TCSC and PSS2B controllers in electric power systems using MOPSO multiobjective algorithm," *Int. Trans. Electr. Energy Syst.*, vol. 2022, pp. 1–18, Nov. 2022, doi: 10.1155/2022/5233620.

[35] A. Nocoń, S. Paszek, and P. Pruski, "Multi-criteria optimization of the parameters of PSS3B system stabilizers operating in an extended power system with the use of a genetic algorithm," *Arch. Sci.*, vol. 32, no. 2, pp. 233–255, 2022, doi: 10.24425/acs.2022.141711.

[36] B. P. Nayak, K. K. Prabhakaran, T. R. Chelliah, and P. Jena, "Investigation of power system stabilizer PSS-3B in a large hydro generating unit," in *Proc. IEEE 2nd Int. Conf. Smart Technol. Power, Energy Control (STPEC)*, Dec. 2021, pp. 1–6, doi: 10.1109/STPEC52385.2021.9718630.

[37] I. A. Ali and A. L. Elshafei, "Model predictive control stabilization of a power system including a wind power plant," *J. Energy Syst.*, vol. 6, no. 2, pp. 188–208, Jun. 2022, doi: 10.30521/jes.997307.

[38] R. Tiwari and T. R. Chelliah, "Design improvement and tuning of excitation system ST5B with PSS3B and coordinated OEL in hydropower plant," *IEEE Trans. Ind. Appl.*, vol. 58, no. 5, pp. 5895–5907, Sep. 2022, doi: 10.1109/TIA.2022.3184667.

[39] K. K. Prabhakaran, R. Tiwari, S. R. Nayak, and T. R. Chelliah, "Performance investigation on damping of active power oscillation in the large hydro-power plant with power system stabilizer," in *Proc. IEEE Int. Conf. Power Electron., Drives Energy Syst. (PEDES)*, Dec. 2020, pp. 1–6, doi: 10.1109/PEDES49360.2020.9379816.

[40] R. T. Elliott, P. Arabshahi, and D. S. Kirschen, "A generalized PSS architecture for balancing transient and small-signal response," *IEEE Trans. Power Syst.*, vol. 35, no. 2, pp. 1446–1456, Mar. 2020, doi: 10.1109/TPWRS.2019.2938205.

[41] S. D. Ahmed, F. S. M. Al-Ismail, M. Shafiullah, F. A. Al-Sulaiman, and I. M. El-Amin, "Grid integration challenges of wind energy: A review," *IEEE Access*, vol. 8, pp. 10857–10878, 2020, doi: 10.1109/ACCESS.2020.2964896.

[42] M. Ranjan and R. Shankar, "A literature survey on load frequency control considering renewable energy integration in power system: Recent trends and future prospects," *J. Energy Storage*, vol. 45, Jan. 2022, Art. no. 103717, doi: 10.1016/j.est.2021.103717.

[43] A. Q. Al-Shetwi, "Sustainable development of renewable energy integrated power sector: Trends, environmental impacts, and recent challenges," *Sci. Total Environ.*, vol. 822, May 2022, Art. no. 153645, doi: 10.1016/j.scitotenv.2022.153645.

[44] S. Niu, Z. Zhang, X. Ke, G. Zhang, C. Huo, and B. Qin, "Impact of renewable energy penetration rate on power system transient voltage stability," *Energy Rep.*, vol. 8, pp. 487–492, Apr. 2022, doi: 10.1016/j.egyr.2021.11.160.

[45] B. B. Adetokun, C. M. Muriithi, and J. O. Ojo, "Voltage stability assessment and enhancement of power grid with increasing wind energy penetration," *Int. J. Electr. Power Energy Syst.*, vol. 120, Sep. 2020, Art. no. 105988, doi: 10.1016/j.ijepes.2020.105988.

[46] M. Bajaj and A. K. Singh, "Grid integrated renewable DG systems: A review of power quality challenges and state-of-the-art mitigation techniques," *Int. J. Energy Res.*, vol. 44, no. 1, pp. 26–69, Jan. 2020, doi: 10.1002/er.4847.

[47] G. S. Chawda, A. G. Shaik, M. Shaik, S. Padmanaban, J. B. Holm-Nielsen, O. P. Mahela, and P. Kaliannan, "Comprehensive review on detection and classification of power quality disturbances in utility grid with renewable energy penetration," *IEEE Access*, vol. 8, pp. 146807–146830, 2020, doi: 10.1109/ACCESS.2020.3014732.

[48] G. S. Chawda, A. G. Shaik, O. P. Mahela, S. Padmanaban, and J. B. Holm-Nielsen, "Comprehensive review of distributed FACTS control algorithms for power quality enhancement in utility grid with renewable energy penetration," *IEEE Access*, vol. 8, pp. 107614–107634, 2020, doi: 10.1109/ACCESS.2020.3000931.

[49] U. Datta, A. Kalam, and J. Shi, "The relevance of large-scale battery energy storage (BES) application in providing primary frequency control with increased wind energy penetration," *J. Energy Storage*, vol. 23, pp. 9–18, Jun. 2019, doi: 10.1016/j.est.2019.02.013.

[50] M. Elsisi, N. Bazmohammadi, J. M. Guerrero, and M. A. Ebrahim, "Energy management of controllable loads in multi-area power systems with wind power penetration based on new supervisor fuzzy nonlinear sliding mode control," *Energy*, vol. 221, Apr. 2021, Art. no. 119867, doi: 10.1016/j.energy.2021.119867.
[51] P. Rokni Nakhi and M. Ahmadi Kamarposhti, "Multi objective design of type II fuzzy based power system stabilizer for power system with wind farm turbine considering uncertainty," *Int. Trans. Electr. Energy Syst.*, vol. 30, no. 4, Apr. 2020, doi: 10.1002/2050-7038.12285.
[52] G. Zhang, W. Hu, D. Cao, Q. Huang, Z. Chen, and F. Blaabjerg, "A novel deep reinforcement learning enabled sparsity promoting adaptive control method to improve the stability of power systems with wind energy penetration," *Renew. Energy*, vol. 178, pp. 363–376, Nov. 2021, doi: 10.1016/j.renene.2021.06.081.
[53] S. Essallah, A. Bouallegue, and A. Khedher, "Integration of automatic voltage regulator and power system stabilizer: Small-signal stability in DFIG-based wind farms," *J. Modern Power Syst. Clean Energy*, vol. 7, no. 5, pp. 1115–1128, Sep. 2019, doi: 10.1007/s40565-019-0539-0.
[54] A. K. Gupta, K. Verma, and K. R. Niazi, "Robust coordinated control for damping low frequency oscillations in high wind penetration power system," *Int. Trans. Electr. Energy Syst.*, vol. 29, no. 5, May 2019, Art. no. e12006, doi: 10.1002/2050-7038.12006.
[55] A. A. Alsakati, C. A. Vaithilingam, J. Alnasseir, K. Naidu, and G. Rajendran, "Transient stability enhancement of grid integrated wind energy using particle swarm optimization based multi-band PSS4C," *IEEE Access*, vol. 10, pp. 20860–20874, 2022, doi: 10.1109/ACCESS.2022.3151425.
[56] A. M. Ilyas, A. Suyuti, I. C. Gunadin, and A. Siswanto, "Optimal power flow the sulselrabar 150 KV system before and after the penetration of wind power plants considering power loss and generation costs," *IOP Conf. Ser., Mater. Sci. Eng.*, vol. 850, no. 1, 2020, Art. no. 012030, doi: 10.1088/1757-899X/850/1/012030.
[57] B. Mustadir Darusman, A. Suyuti, and I. C. Gunadin, "Small signal stability analysis of wind turbine penetration in sulselrabar interconnection system," *J. Phys., Conf.*, vol. 1090, Sep. 2018, Art. no. 012034, doi: 10.1088/1742-6596/1090/1/012034.
[58] Z.-M. Zhai, L.-W. Kong, and Y.-C. Lai, "Emergence of a resonance in machine learning," *Phys. Rev. Res.*, vol. 5, no. 3, Aug. 2023, Art. no. 033127, doi: 10.1103/physrevresearch.5.033127.
[59] Z.-M. Zhai, M. Moradi, L.-W. Kong, B. Glaz, M. Haile, and Y.-C. Lai, "Model-free tracking control of complex dynamical trajectories with machine learning," *Nature Commun.*, vol. 14, no. 1, p. 5698, Sep. 2023, doi: 10.1038/s41467-023-41379-3.
[60] R. Liu, Y. Mo, Y. Lu, Y. Lyu, Y. Zhang, and H. Guo, "Swarm-intelligence optimization method for dynamic optimization problem," *Mathematics*, vol. 10, no. 11, p. 1803, May 2022, doi: 10.3390/math10111803.
[61] M. Djalal, "Optimal power system stabilizer design using craziness particle swarm optimization in sulselrabar system," *Przeglad Elektrotechniczny*, vol. 1, no. 10, pp. 78–83, Sep. 2021, doi: 10.15199/48.2021.10.15.
[62] K. Zervoudakis and S. Tsafarakis, "A mayfly optimization algorithm," *Comput. Ind. Eng.*, vol. 145, Jul. 2020, Art. no. 106559, doi: 10.1016/j.cie.2020.106559.
[63] E. V. Fortes, L. F. B. Martins, M. V. S. Costa, L. Carvalho, L. H. Macedo, and R. Romero, "Mayfly optimization algorithm applied to the design of PSS and SSSC-POD controllers for damping low-frequency oscillations in power systems," *Int. Trans. Electr. Energy Syst.*, vol. 2022, pp. 1–23, Apr. 2022, doi: 10.1155/2022/5612334.
[64] A. A. Eid, A. M. A. Soliman, and M. A. Mehanna, "Optimize gain values of PI-controller for active power filter using mayfly algorithm," *Int. J. Renew. Energy Res.*, vol. 12, no. 4, pp. 1727–1735, 2022, doi: 10.20508/ijrer.v12i4.13413.g8597.
[65] G. Lei, X. Chang, Y. Tianhang, and W. Tuerxun, "An improved mayfly optimization algorithm based on median position and its application in the optimization of PID parameters of hydro-turbine governor," *IEEE Access*, vol. 10, pp. 36335–36349, 2022, doi: 10.1109/ACCESS.2022.3160714.
[66] R. Sadiq, Z. Wang, C. Y. Chung, C. Zhou, and C. Wang, "A review of STATCOM control for stability enhancement of power systems with wind/ PV penetration: Existing research and future scope," *Int. Trans. Electr. Energy Syst.*, vol. 31, no. 11, Nov. 2021, Art. no. e13079, doi: 10.1002/2050-7038.13079.
[67] H. Setiadi, N. Mithulananthan, R. Shah, M. R. Islam, A. Fekih, A. U. Krismanto, and M. Abdillah, "Multi-mode damping control approach for the optimal resilience of renewable-rich power systems," *Energies*, vol. 15, no. 9, p. 2972, Apr. 2022, doi: 10.3390/en15092972.
[68] H. Saadat, *Power System Analysis*. New York, NY, USA: McGraw-Hill, 2009.
[69] P. S. Kundur and O. P. Malik, *Power System Stability and Control*. New York, NY, USA: McGraw-Hill, 2022.
[70] H. Setiadi, F. Arrazi, M. Abdillah, and A. U. Krismanto, "Smart DIPSS for dynamic stability enchancement on multi-machine power system," *Indonesian J. Electr. Eng. Informat. (IJEEI)*, vol. 10, no. 1, pp. 43–50, Mar. 2022, doi: 10.52549/ijeei.v10i1.3429.
[71] I. Manuaba, U. Udayana, M. Abdillah, R. Zamora, H. Setiadi, U. Pertamina, and U. Airlangga, "Adaptive power system stabilizer using kernel extreme learning machine," *Int. J. Intell. Eng. Syst.*, vol. 14, no. 3, pp. 468–480, Jun. 2021, doi: 10.22266/ijies2021.0630.39.
[72] Z.-M. Gao, J. Zhao, S.-R. Li, and Y.-R. Hu, "The improved mayfly optimization algorithm," *J. Phys., Conf.*, vol. 1684, no. 1, Nov. 2020, Art. no. 012077, doi: 10.1088/1742-6596/1684/1/012077.

MUHAMMAD RUSWANDI DJALAL was born in Ujung Pandang, in March 1990. He received the bachelor's degree in energy engineering from the State Polytechnic of Ujung Pandang, Makassar, Indonesia, in 2012, and the master's degree in electrical engineering from the Institut Teknologi Sepuluh Nopember, Surabaya, Indonesia, in 2015, where he is currently pursuing the Ph.D. degree with the Department of Electrical Engineering through the Beasiswa Pendidikan Indonesia (BPI) Scholarship Program. Alongside his academic pursuits, he was a Lecturer in energy engineering with the Department of Mechanical Engineering, State Polytechnic of Ujung Pandang, where he is also a member of the Center for Sustainable Energy and Smart Grid Applications (CoSESGA) Research Group. His research interests include power system stability, renewable energy, and artificial intelligence (AI).

IMAM ROBANDI was born in Kebumen, in August 1963. He received the bachelor's degree in electrical engineering from the Institut Teknologi Sepuluh Nopember, Surabaya, Indonesia, in 1989, the master's degree from the Department of Electrical Engineering, Institut Teknologi Bandung, Bandung, Indonesia, in 1995, and the Ph.D. degree from the Department of Electrical Engineering, Tottori University, Japan, in 2002. He is currently a Professor with the Department of Electrical Engineering, Institut Teknologi Sepuluh November. He specializes in the application of artificial intelligence in electrical power system engineering. In addition, he was the Head of the Power System Operation and Control Laboratory, Department of Electrical Engineering, Institut Teknologi Sepuluh November. In 2008 and 2011, he was a Visiting Professor with Tottori University. In 2010, he was also a Visiting Professor with Kumamoto University. Currently, he holds the position of the Chairperson of the Board of Professors with the Institut Teknologi Sepuluh Nopember. Additionally, he serves as the Deputy General Chair for the Indonesian Professors Council Forum (FDGBI) (2024–2025).

MOHAMAD ALMAS PRAKASA was born in Brebes, in September 1999. He received the bachelor's degree from the Department of Electrical Engineering, Universitas Negeri Semarang (UNNES), Semarang, Indonesia, in 2017, and the master's degree from the Department of Electrical Engineering, Institut Teknologi Sepuluh Nopember (ITS), Surabaya, Indonesia, in 2021, with a Fast-Track Scholarship Program, where he is currently pursuing the Ph.D. degree with the Department of Electrical Engineering through the PMDSU Scholarship Program. He is a member of the Power System Operation and Control (PSOC) Laboratory. His research interests are artificial intelligence application to electrical power systems, especially to dynamic stability and RES microgrid optimization.